MATHEMATICAL MODELLING AND SURVIVAL PREDICTION IN CANCER

Anni S. Halkola

TURUN
YLIOPISTO
UNIVERSITY
OF TURKU

MATHEMATICAL MODELLING AND SURVIVAL PREDICTION IN CANCER

Anni S. Halkola

Supervised by

Associate prof. Kalle Parvinen, PhD

Department of Mathematics and Statistics
University of Turku
Turku, Finland

Advancing Systems Analysis Program
International Institute for Applied Systems Analysis (IIASA)
Laxenburg, Austria

Prof. Tero Aittokallio, PhD

Institute for Molecular Medicine Finland
(FIMM), University of Helsinki
Helsinki, Finland

Institute for Cancer Research
Oslo University Hospital
Oslo, Norway

Oslo Centre for Biostatistics and Epidemiology (OCBE), University of Oslo
Oslo, Norway

Reviewed by

Associate prof. Harri Lähdesmäki, D.Sc. (Tech)

Department of Computer Science
Aalto University
Espoo, Finland

Research Associate Alvaro Köhn-Luque, PhD

Institute of Basic Medical Sciences
University of Oslo
Oslo, Norway

Opponent

Prof. Joel S. Brown, PhD

Moffitt cancer center
Tampa, FL, USA

University of Illinois
Chicago, USA

The originality of this publication has been checked in accordance with the University of Turku quality assurance system using the Turnitin OriginalityCheck service.

To anyone affected by cancer
(so basically everyone)

ABSTRACT

Cancer is one of the leading causes of death, thus opening a vast need for extensive research and insights. The survival prospects, along with treatment benefits and costs (economical or health-related), can be predicted with tools from mathematical modelling and regression analysis. Promising results have been gained on suggesting mono- and combination therapies, that could potentially improve the treatment strategies. Furthermore, multiple biological features have been recognized as important predictors of treatment outcome. However, since cancer remains a challenging and unpredictable enemy, the need for more effective and personalized predictions and treatment suggestions remains.

In this dissertation, various modelling approaches were used to predict cancer behavior, treatment outcomes and patient survival. An ordinary differential equation model was developed to investigate the changes in the cancer cell density as different treatment regimen were applied. In addition, we included the immune system along with immunotherapy, since the immune response is an important part of cancer development and has a potential to eradicate tumors. It was noted, that an adaptive treatment resulted in lower cancer burden and less time in treatment. In addition, combination treatments (immunotherapy with either chemo- or targeted therapy) generally resulted in smaller cancer burden than monotherapies, however, the potential additional side effects of two therapies have to be considered.

A metapopulation model was developed for the cancer development, in which the focus was on emergence of angiogenesis and cancer cell emigration. We investigated, in which conditions cancer cells would become angiogenic with or without treatments (anti-angiogenic, cytotoxic or combination). In general, angiogenesis contribution was desired quality for cancer cells, if no anti-angiogenic treatment was administrated. With anti-angiogenic treatment, angiogenesis diminished, however the risk of resistance against anti-angiogenic treatment also increased.

Two new regression methods were developed with focus on survival prediction. A greedy budget-constrained Cox regression (Greedy Cox) utilizes L_2-penalty and considers the cost of selected parameters. It was also compared to LASSO selection (L_1). Optimal Subset CArdinality Regression (OSCAR) method was developed with L_0-pseudonorm penalty to provide sparse models. The costs of measuring the selected model features were also considered in comparison to prediction accuracy. The methods were validated on clinical prostate cancer data and it was noted that a comparable level of prediction accuracy was already reached with a few parameters,

resulting in relatively low costs. All of the investigated methods also selected reasonable, cancer-related parameters such as prostate specific antigen (PSA).

Taken together, this dissertation provides a comprehensive research of novel tools for modelling and predicting cancer behavior and patient survival. Important hallmarks of cancer development, such as immune response and angiogenic switch have been included along with corresponding treatments that have potential to change the traditional treatment regimens.

KEYWORDS: cancer, killer T-cells, mathematical modelling, personalized medicine, immunotherapy, anti-angiogenic treatment, cytotoxic treatment, targeted treatment, combination therapy, side-effects, tumor microenvironment, metapopulation modelling, cost optimization, survival prediction, Cox regression, prostate cancer, feature selection, L_0-pseudonorm

TIIVISTELMÄ

Syöpä on yksi yleisimmistä kuolinsyistä aiheuttaen tarpeen laajalle ja kattavalle tutkimukselle. Selviytymismahdollisuuksia sekä hoitojen hyötyjä ja haittoja (ekonomisia tai terveydellisiä) voidaan ennustaa hyödyntäen matemaattista mallintamista ja regressioanalyysiä. Lupaavia teoreettisia ehdotuksia onkin jo saatu esimerkiksi mono- ja kombinaatiohoidoista, jotka voisivat potentiaalisesti parantaa hoitostrategioita. Lisäksi analyysien avulla on tunnistettu useita biomarkkereita, jotka ennustavat hoitovastetta. Tästä huolimatta syöpä on edelleen hankala ja ennalta-arvaamaton vastustaja, jota vastaan tarvitaan yhä tehokkaampia ja yksilöllisempiä vaste-ennusteita ja hoitoja.

Tässä väitöskirjassa on käytetty erilaisia lähestymistapoja syövän käyttäytymisen, hoitovasteiden ja potilaan selviytymisen ennustamiseen. Differentiaaliyhtälöihin perustuvalla mallilla tutkittiin, kuinka syövän määrä muuttuu erilaisten hoitojen ja hoitoaikataulujen seurauksena. Lisäksi malliin sisällytettiin mekanismit immuunivasteelle ja immunohoidolle, koska immuunipuolustuksella on tärkeä rooli syövän kehittymisessä ja tuhoamisessa. Havaittiin, että adaptiivinen hoito tuotti pienemmät syöpämäärät ja hoitoa tarvittiin vähemmän. Lisäksi kombinaatiohoidot (immunohoito joko kemoterapian tai targetoidun hoidon kanssa) aiheuttivat yleensä pienemmät syöpämäärät kuin hoidot erikseen annettuina. Kombinaatiohoitojen yhteydessä on kuitenkin huomioitava, että kahdesta päällekkäisestä hoidosta voi aiheutua ylimääräisiä sivuvaikutuksia.

Toisessa lähestymistavassa syöpää mallinnettiin metapopulaatiomallin avulla. Tässä keskityttiin angiogeneesin kehittymiseen ja solujen liikkumiseen paikasta toiseen (emigraatio). Mallin avulla tutkittiin, missä olosuhteissa syöpäsolut muuttuvat angiogeenisiksi ja miten hoidot vaikuttavat (antiangiogeeninen, sytotoksinen tai kombinaatiohoito). Yleisesti syöpäsolujen kannalta oli hyödyllistä edistää angiogeneesiä, jos antiangiogeenistä hoitoa ei ollut. Hoidon kanssa angiogeneesi hävisi, mutta toisaalta myös riski hoitoresistenttiydelle kasvoi.

Lisäksi kehitettiin uusia regressiometodeita erityistesti potilaan selviytymistodennäköisyyden ennustamiseen. Greedy Cox (a greedy budget-constrained Cox regression) metodi tuottaa regressiomalleja, joissa muuttujien määrää rajoitetaan L_2-normin avulla. Greedy Cox huomioi, kuinka paljon piirteiden mukaan ottaminen maksaisi ja metodille voidaan antaa käytettävissä oleva budjetti. Greedy Coxia myös verrattiin LASSO-pohjaiseen mallinvalintaan (L_1-normi rajoittajana). Uusi metodi OSCAR (Optimal Subset CArdinality Regression) kehitettiin hyödyntäen L_0-pseu-

Anni S. Halkola

donormia muuttujien määrän rajoittamisessa. Lisäksi valittujen muuttujien aiheuttama hinta laskettiin ja verrattiin, miten se suhteutui mallin ennustustarkkuuteen. Kaikki esitetyt metodit validoitiin kliinisellä eturauhassyöpäaineistolla. Metodit tuottivat hyvän ennustetarkkuuden jo pienellä määrällä muuttujia, jolloin myös hinta pysyi matalampana. Metodit myös valitsivat järkeviä, (eturauhas)syöpään yhdistettäviä parametreja kuten prostataspesifinen antigeeni (PSA).

Tämä väitöskirja tarjoaa siis kattavan valikoiman uusia välineitä syövän käytöksen ja potilaan selviytymistodennäköisyyden ennustamiseen. Tutkimuksessa huomioitiin tärkeitä syövän osa-alueita, kuten immuunivaste ja angiogeneesin kehittyminen sekä näihin liittyvät hoidot, joilla on mahdollisuus muuttaa perinteisiä hoitokäytäntöjä.

ASIASANAT: syöpä, tappaja T-solut, matemaattinen mallintaminen, yksilöllinen lääkehoito, immunohoito, anti-angiogeeninen hoito, sytotoksinen hoito, targetoitu hoito, kombinaatiohoito, sivuvaikutukset, syövän mikroympäristö, metapopulaatiomalli, hintaoptimointi, selviämisen ennustaminen, Cox-regressio, eturauhassyöpä, piirteiden valinta, L_0-pseudonormi

Acknowledgements

Table of Contents

Abbreviations

AGEGRP	Age group
ALB	Albumin
ALP	Alkaline phosphatase
APM-L_0	Augmented penalized minimization-L_0
AST	Aspartate aminotransferase
BMI	Body mass index
CA	Calcium
CARs	Chimeric antigen receptors
CHF	Congestive heart failure
CRAN	Central R Archive Network
CREAT	Creatinine
CTLA4	Cytotoxic T-lymphocyte antigen-4
B-PVKT	Perusverenkuva ja trombosyytit (Basic blood count and thrombocytes, here includes HB, HEMAT, RBC, WBC and PLT)
DBDC	The double bundle method
DC function	Difference of two Convex functions
FGFs	Fibroblast growth factors
HB	Hemoglobin
HEMAT	Hematocrit
LASSO	Least absolute shrinkage and selection operator
LDH	Lactate dehydrogenase
LMBM	The limited memory bundle method
LYMperLEU	Ratio of lymphocytes and leukocytes
mCRPC	Metastatic castration-resistant prostate cancer
MG	Magnesium
NA	Sodium
NEU	Neutrophils
NEUperLEU	Ratio of neutrophils and leukocytes
NP hard	Nondeterministic polynomial hard
ODE	Ordinary differential equation
OSCAR	Optimal Subset CArdinality Regression
PDGFs	Platelet derived growth factors
PD-1	Programmed cell death protein 1

PD-L1	Programmed death ligand
PLT	Platelets
PSA	Prostate-specific antigen
TYKS	Turun yliopistollinen keskussairaala (Turku University Hospital)
VEGF	Vascular endothelial growth factor
WBC	White blood cells

List of Original Publications

This dissertation is based on the following original publications, which are referred to in the text by their Roman numerals:

I   Anni S. Halkola, Kalle Parvinen, Henna Kasanen, Satu Mustjoki, Tero Aittokallio. Modelling of killer T-cell and cancer cell subpopulation dynamics under immuno- and chemotherapies. Journal of Theoretical Biology, 2020; 488: 110136.

II   Anni S. Halkola, Tero Aittokallio, Kalle Parvinen. Tumor microenvironment as a metapopulation model: The effects of angiogenesis, emigration and treatment modalities. Journal of Theoretical Biology, 2022; 545: 111147.

III   Mika Murtojärvi, Anni S. Halkola, Antti Airola, Teemu D. Laajala, Tuomas Mirtti, Tero Aittokallio, Tapio Pahikkala. Cost-effective survival prediction for patients with advanced prostate cancer using clinical trial and real-world hospital registry datasets. International Journal of Medical Informatics, 2020; 133: 104014.

IV   Anni S. Halkola, Kaisa Joki, Tuomas Mirtti, Marko M. Mäkelä, Tero Aittokallio, Teemu D. Laajala. OSCAR: Optimal subset cardinality regression using the L0-pseudonorm with applications to prognostic modelling of prostate cancer. Submitted for publication.

The original publications have been reproduced with the permission of the copyright holders.

1 Introduction

Cancer is one of the main causes of death with more than 19 million new cases per year [1]. Mathematical and prognostic survival modelling offer insights into individualized patient care and treatment outcomes.

Tumors have their individual, genetically, functionally or epigenetically distinct cancer cell populations that develop throughout the disease progression and in response to the treatments. Understanding the dynamic evolutionary processes that undergo before and during treatments, enables the prediction of treatment outcomes and eases the optimization and personalization of cancer treatment. Mathematical modelling has already provided some insights into treatment sensitivity and resistance along with suggestions of mono- or combination therapies [2; 3; 4; 5; 6; 7; 8].

Modelling aids the understanding of underlying dynamics and investigation of the qualitative possibilities of different treatment regimens. In addition, data-based prediction is crucial in the cancer care to predict the risk of death or cancer recurrence, and to identify patients that would benefit from a specific treatment. The treatment outcome is predicted by utilizing laboratory tests. However, depending on the cancer type, the process may involve numerous tests and the healthcare costs often rise. The prognostic prediction by survival models (here Cox's regression [9]), especially penalized regression, allows the selection of most prominent predictors in the assessment of treatment outcome with respect to survival (e.g. overall survival or progress free survival). Thus, the model sparsity enables pruning unnecessary predictors along with their costs.

This dissertation includes three chapters that focus on the different approaches that were used in the cancer modelling and outcome prediction. The chapters summarize the results and related research of this work. In Chapter 2 the focus is on Publication I, in which cancer was modelled with ordinary differential equations. The aim was to model the dynamics between immune system and cancer, as well as to predict possible qualitative outcomes of different treatment modalities. Thus, the model includes the immune system (active killer T-cells) and an immunotherapy mechanism that boosts the immune response in case cancer has started to prevent the T-cells' efficacy. The Chapter 2 is further divided into sections that offer a review on the subject (Section 2.1), an overview to the presented model (Section 2.2) and the results (Section 2.3).

Chapter 3 focuses on the metapopulation modelling approach presented in Publication II. The aim was to gain insights into underlying evolutionary dynamics that lead to cancer development. The cancer cells had three strategies (contribution to angiogenesis, emigration and treatment resistance) that evolved based on the current living conditions that were determined by the cells, resource availability and treatments. Angiogenesis mechanism was included along with anti-angiogenic treatment and treatment resistance. Chapter 3 is divided into literature review (Section 3.1), the model and results overviews (Sections 3.2 and 3.3 respectively).

Chapter 4 summarizes both Publication III and IV as both were based on the Cox regression [9] and predicting the treatment outcome on prostate cancer data cohorts. In Publication III, the aim was to offer a method to efficiently predict treatment outcomes (e.g. overall survival or progress-free survival), while considering also the costs that the model variables would have in practice. Two algorithms were tested: LASSO-based selection and a greedy budget-constrained Cox regression (Greedy Cox). In the latter, the budget was considered within the algorithm. In Publication IV, the aim was to produce prognostic models while offering different levels of model sparsity. The proposed OSCAR method implemented penalization with L_0-pseudonorm, which is less studied in penalized regression due to its discontinuous and nonconvex nature. Chapter 4 is divided into three sections, starting with literature review (Section 4.1). The second section (Section 4.2) is an overview on materials and methods, which is further divided into introduction of data and methods in Publications III and IV. The third section (Section 4.3) gives an overview on the results of Publications III and IV.

In Chapter 5 the results from all publications are discussed with ideas for future research. Finally, Chapter 6 concludes the dissertation with a short summary.

2 Cancer cell population model with immune system

In Publication I, cancer has been modelled with an ordinary differential equation (ODE) model. The aim was to model the dynamic competition between the immune system and cancer, and to gain insights into qualitative behavior of the cells under and after different treatment choices. Thus, in addition to cancer cells, the immune system was included in the form of active killer T-cells. The inclusion of T-cells enabled the inclusion of immunotherapy. We also modelled the effects of targeted therapy and chemotherapy and investigated the treatments as monotherapies or as a combination. See Figure 1 for the components and their interactions. The cancer cell type was determined by the cell qualities like resource consumption rate, aggressiveness against T-cells and the effectiveness of treatments. We investigated a few different cancer cell types and predicted how different treatment regimens affected the cell densities.
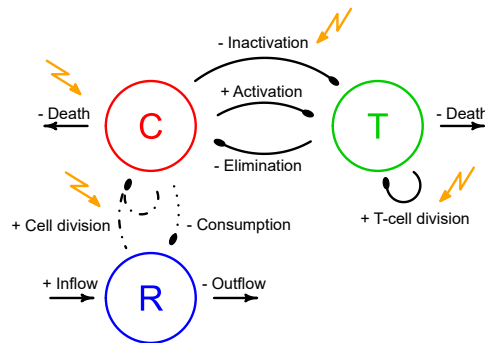
Figure 1. The interactions of (cancer) cells (C), active killer T-cells (T) and resources (R) (e.g. glucose). The ellipses point the affected entity with the sign indicating the change in the density. Lightning bolt arrows indicate the treatments: chemotherapy affects the cells divisions, targeted therapy affects the cancer cell death and immunotherapy affects the inactivation of T-cells. (Adopted with permission from Publication I: Fig. 1.)

2.1 Literature review

As cancer remains one of the most common causes of death, it is also a solid interest for mathematical modelling. In addition to dynamic modelling of the cancer cells

or density, the models may also suggest theoretical therapy regimens and predict possible treatment outcomes. Similarly to our model in Publication I, many models assume that cancer has survived the early stages and has reached a considerable, possibly detectable, size. This assumption justifies that the tumor can be modelled as a continuous variable, enabling the use of differential equations in the modelling of the cancer dynamics. For example, Fassoni et al. [10] proposed an ODE model for chronic myeloid leukemia. They consider multiple different sub-models with different functional interactions between cells. Letellier et al. [11] included four ODEs in their model (host, immune, tumor and endothelial cells). Also others, such as [12; 13; 7] utilized differential equations in their cancer modelling. Pinho et al. [12] had five differential equations for normal, cancer and endothelial cells along with chemotherapy and anti-angiogenic agents. Also Yonucu et al. [13] focused on the effects of anti-angiogenic and chemotherapies with ODEs for tumor, vasculature, interstitial fluid pressure and therapy agents. Zhang et al. [7] considered abiraterone therapy in prostate cancer model with three cancer cell types that differ in their androgen relation. They modelled the system as Lotka-Volterra equations including an interaction matrix of the different cell types. Louzoun et al. [5] modelled pancreatic cancer with four ODEs including cancer cells, host cells, T-cells and the ratio of two macrophage phenotypes.

Many of the above mentioned models included some form of normal or host cells along with the cancer cells. In our ODE model, the cell type is general, though mainly thought to be cancerous in the presented analyses. However, the cell type may be modified by selecting cell type specific parameter values indicating a normal cell behavior. For example, the proliferation rate may be decreased or the normal apoptosis rate increased. Additionally, the interaction with the active killer T-cells may be selected to be small or non-existent.

In addition to differential equations, other approaches have been considered in research [6; 8]. Opposite to the assumption that cancer has reached a considerable size, other models have considered only a single cell or a few cells. These early stages may be modelled by branching processes. Avanzini and Antal [14] proposed a branching process model to investigate the formation and evolution of metastatic lesions based on the size of the primary tumor. Also Bozic and Nowak [3] focused on metastatic cancer and model a lesion as a branching process with possibility of treatment resistance. Bozic et al. [2] investigated the need of targeted combination therapy with a model based on multitype branching process. Kozłowska et al. [15] utilized a stochastic multitype branching process in which cancer cells can acquire multiple resistance mechanisms.

Various other approaches have been used as well, for example, cellular automata by Lai et al. [16] and Alarcón et al. [17]. Komarova, Burger and Wodarz [18] used a stochastic birth-death process model to predict the relapse and emergence of treat-

ment resistance against a targeted therapy (ibrutinib). Fischer, Vázquez-García and Mustonen [4] used a Wright-Fisher model with stochastic optimal control to investigate adaptive therapies in case of treatment resistance. A metapopulation modelling approach has been used in Publication II (see Chapter 3).

2.1.1 Immune system and immunotherapy in modelling

Many cancer models do not include the immune system, which has a significant role in the development and life cycle of cancer. In our model in Publication I, we have included the immune system in the form of active killer T-cells, that are an important part of the immune response. Fassoni et al. [10] included the immune system cells along with quiescent and proliferating cancer cells. Similarly to our model, they considered one type of immune cells (e.g., natural killer cells). However, in their model, cancer cells only affect the immune cell density positively by recruiting, whereas in our model the cancer cells may also decrease the T-cell density. This negative effect on the immune system justifies the use of immunotherapy and enables its inclusion in our model. Fassoni et al. considered targeted therapy (tyrosine kinase inhibitors) that affects only proliferating cancer cells. Letellier et al. [11] modelled the immune cells, however, similarly to Fassoni et al. they did not include immunotherapy. Instead, their focus was on the combination of anti-angiogenic treatment and chemotherapy.

In our model in Publication I the active killer T-cells are produced based on the antigen delivery from dying cancer cells [19; 20; 21]. The active killer T-cells are in contact with the cancer cells causing the death of the latter. However, we included a mechanism in which the cancer cells may cause inactivation of the T-cells leading to ineffective T-cells. This model mechanism is based on the binding between programmed death-ligand (PD-L1) on the cancer cell surface and its receptor programmed cell death protein 1 (PD-1) on the T-cell surface [19]. The binding prevents the T-cell function, however, this may be prevented by a form of immunotherapy, immune-checkpoint inhibitors (e.g., nivolumab and pembrolizumab). Such a immune-checkpoint inhibitor is, for example, anti-PD-L1, which binds to PD-L1 preventing the connection with PD-1, or anti-PD-1 which binds to PD-1 leading to similar results [22; 23]. We included this mechanism in our model in Publication I.

Since the immune response is a complex system, the PD-L1/PD-1 interaction is not the only mechanism that may be targeted by immunotherapy. The immune response requires the antigen delivery, antigen presentation to the immune system, priming and activation of T-cells, trafficking and infiltration of T-cells into tumors and recognition and killing of cancer cells [19].

Chemotherapy, radiation and targeted therapies might enhance the antigen delivery by increasing the cancer cell death. Antigen presentation can be promoted by im-

munotherapy vaccines. Cancer cells may affect the activation of T-cells, which may be inhibited by CTLA4 (a negative regulator of T-cells). This interaction is targeted by anti-CTLA4 antibodies (e.g. ipilimumab) [24]. The trafficking and infiltration of T-cells into tumor microenvironment might also be compromised. Treatments like anti-VEGF (bevacizumab) and B-Raf inhibitors (vemurafenib) may enhance the tumor infiltration [25; 26]. In CAR-T immunotherapy, CARs (chimeric antigen receptors) are produced from patient's T-cells and modified to adhere and attack cancer cells [27]. Also combinations of multiple immunotherapies have been considered [28; 29; 30; 31].

2.1.2   Treatment modelling

In addition to immunotherapy, in Publication I, we considered also chemotherapies (e.g. dacarbazine or temozolomide) and targeted therapies (e.g. BRAF or C-KIT inhibitors). Since the cytostatic treatment damages the cell cycle benchmarks [32], rapidly dividing (cancer) cells have less time to recover, thus making them more vulnerable for the treatment. Targeted treatment recognizes specific proteins, thus allowing targeted elimination of only cells with the target protein. These are more traditional treatment modalities and as such are more widely considered in the cancer models. For example, Fassoni et al. [10] modelled targeted therapies, and Pinho et al. [12] and Yonucu et al. [13] modelled chemotherapies. In our model in Publication I, we used these therapies also in a combination with immunotherapy.

Other mono- or combination therapies can also be considered in mathematical modelling. Depending on the scenario and cancer type, one could consider, for example, hormone therapy like abiraterone therapy in prostate cancer [7] or radiation therapy. Also anti-angiogenic treatment has been used in cancer treatment [33; 34; 35] and we have modelled such treatment mechanism in Publication II (see Chapter 3).

2.2   Model

The minimum model consists of three ordinary differential equations: resources (e.g. glucose), active killer T-cells and cancer cells. More cell populations could be included by adding a differential equation for each with cell type specific parameter values.

2.2.1   Resources

Since the cells require resources for their proliferation, we included the amount of resources as a part of the competitive situation. Resources flow in to and out of the tumor microenvironment following chemostat dynamics in the absence of resource

consuming cells [36]. However, in addition to normal flow through the region, the cells consume the resources following the law of mass action [37]. Thus the differential equation for resources is

$$\frac{dR}{dt} = \underbrace{\lambda(\hat{R} - R)}_{\text{Flow}} - \underbrace{\left(1 - w\frac{\sum\limits_{j} C_j}{1 + \sum\limits_{j} C_j}\right) \sum\limits_{j} \alpha(s_{C_j})RC_j}_{\text{Consumption by cells}}, \quad (1)$$

where λ is the relative flow speed, $\hat{R}$ is the baseline resource inflow and C_j is the density of type j cells. Cells are assumed to restrict each other's resource consumption, for example, by increasing the distance between veins [38], and w is the maximum proportion at which cells limit each other's resource consumption.

Here s_{C_j} is the proliferation strategy of the cell type C_j and $\alpha(s_{C_j})$ is the corresponding resource consumption rate. The rate $\alpha(s_{C_j})$ is an increasing function with lower and upper limits (see Figure 2). The lower limit is assumed since cells require at least some resources to maintain themselves, and the upper limit is assumed since the cells cannot consume resources infinitely fast.
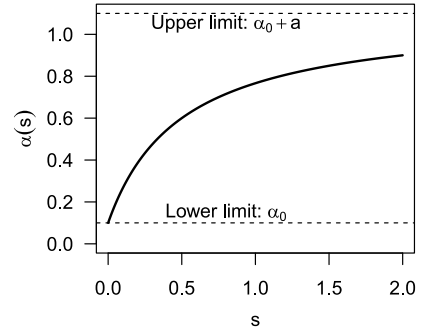
Figure 2. The form of the resource consumption rate $\alpha(s_{C_j})$ with the lower and upper limits for the parameter values presented in the Publication I.

2.2.2 Cancer cells

Cancer cell dynamics are determined by the proliferation proportional to the resource consumption and death by normal apoptosis, drugs or active killer T-cells. The cells attempt to divide based on their resource consumption:

$$\gamma\alpha(s_{C_i}) \left(1 - w\frac{\sum\limits_{j} C_j}{1 + \sum\limits_{j} C_j}\right) RC_i, \quad (2)$$

where γ is the conversion coefficient. However, the division may not be successful in the presence of cytostatic drugs that interfere with the mitosis. Thus, the division fails and the cells face death with the probability p_i. Accordingly, the division proceeds with the probability $(1 - p_i)$. The cytostatic treatments affect rapidly dividing

cells more than cells that hardly divide, therefore, the probability p_i depends on the proliferation strategy s_i:

$$p_i = \frac{s_i}{1 + s_i} H_p, \tag{3}$$

where H_p is the dose-response effect (Hill equation [39]) for the cytostatic drug. It is assumed for simplicity that the drug concentration is a positive constant during the treatment periods and zero afterwards.

In addition to cytostatic drugs, the division may be prevented by the microenvironment carrying capacity, assumed to depend on, e.g., limitations of space. Thus, aggregating the above factors, a successful division happens with the likelihood

$$(1 - p_i) \left(1 - \frac{\sum_j C_j}{K} \right), \tag{4}$$

where K is the carrying capacity.

Cancer cells of the type i die by natural apoptosis with the death rate μ_i. This rate is increased by the rate β_i in case a targeted drug is administered. Now $\beta_i = 0$, if the cell type i is resistant to the targeted treatment. Similarly to cytostatic treatment, the targeted drug concentration is considered to be a constant during the treatment period, and thus the rate β_i is also considered to be a constant. In addition to drugs, active killer T-cells may cause cancer death as the proportion θ of the T-cells enters the cancer microenvironment and proceeds to attack the cancer cells with the rate ξ_i. However, if a cancer cell type lacks the specific antigen, the T-cells ignore the cells and $\xi_i = 0$. Thus, we obtain the following differential equation for the cancer cells:

$$\frac{dC_i}{dt} = \underbrace{\gamma \alpha(s_{C_i}) \left(1 - w \frac{\sum_j C_j}{1 + \sum_j C_j} \right) RC_i}_{\text{Proliferation attempt}} \underbrace{\left((1 - p_i) \left(1 - \frac{\sum_j C_j}{K} \right) \underbrace{-p_i}_{\text{Failure and death}} \right)}_{\text{Proliferation succeeds}}$$

$$\underbrace{-\mu_i C_i - \beta_i C_i - \xi_i C_i \theta T}_{\text{Death}}. \tag{5}$$

2.2.3 Immune system

The killer T-cells are activated in relation to the antigens delivered by the dying cancer cells. The amount of antigen delivery rate d_C depends on the cancer cell death as the dying cancer cells deliver antigens to the blood stream [19]. The rate d_C considers the normal cancer cell apoptosis, death by T-cells and death due to the

targeted or cytostatic drugs. The killer T-cell activation rate $h(d_C)$ is assumed to be sigmoid function (Fig. 3a) since the activation may not be initiated properly with small amount of antigen delivery due to the insufficient signal [40]. Furthermore, the T-cell activation rate $h(d_C)$ has the maximum value of m.
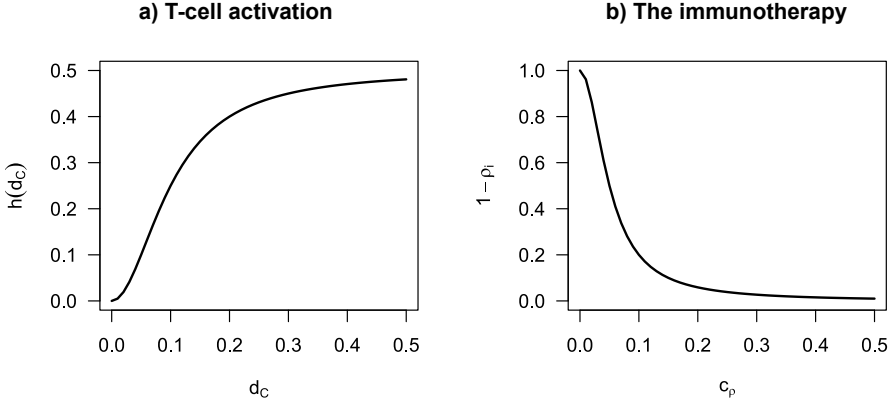
Figure 3. a) The form of the killer T-cell activation $h(d_C)$. b) The form of the overall effect of the immunotherapy ρ_i.

The activated T-cells attempt division with the rate α_T. However, cytostatic drugs may cause division failure and subsequent cell death with the probability p_T. Thus the dividing T-cells die with the rate $\alpha_T p_T$ and succeed to divide with the rate $\alpha_T(1-p_T)$. The activated T-cells may also die due to natural apoptosis (μ_T). The proportion θ of the active killer T-cells enters the microenvironment. Those T-cells then proceed to kill the cancer cells that have the specific antigen. The cancer cells may also make the T-cells ineffective with the cell type specific rate φ_i, while the immunotherapy (ρ_i) counteracts the action. The effect function of immunotherapy ρ_i is sigmoidal, following the general form of dose-response curves [39] (Fig. 3b). For the effect of immunotherapy, $\rho_i = 1$ is desired as it would lead to full prevention of PD-1/PD-L1 interaction between type i cancer cells and T-cells ($(1 - \rho_i)\varphi_i C_i \theta T = 0$). As with the other treatments, the concentration of the immunotherapy drug is set to a positive constant or zero depending on whether the patient is on a treatment period or on a treatment break (drug holiday). Finally, the immune system has self-regulation [41] with the rate δ. Thus, we obtain the following differential equation for the active killer T-cells:

$$\frac{dT}{dt} = \underbrace{h(d_C)}_{\text{Activation}} \underbrace{+\alpha_T(1 - p_T)T}_{\text{Proliferation}} \underbrace{-\mu_T T - \alpha_T p_T T}_{\text{Death}} \underbrace{-\frac{\delta}{2}T^2}_{\text{Self-regulation}} \underbrace{-\sum_i (1 - \rho_i)\varphi_i C_i \theta T}_{\text{PD-1/PD-L1 interaction}}.$$

$$(6)$$

9

2.3 Results

We investigated several case studies, i.e. virtual patients characterized by patient specific model parameters. We focused on the immunotherapy effect either as a monotherapy or in a combination with targeted and chemotherapies. The immune-checkpoint inhibitors generally used in practice include, for example nivolumab administered fortnightly or pembrolizumab which is given every 3rd week. However, these schedules may not be optimal and thus the timing and duration of treatment remains under investigation.

Since the main focus is on the immune system, the virtual patients differed in their T-cell functions. We altered the maximum activation rate of killer T-cells as well as the birth rate of the activated T-cells along with the interaction rates between T-cells and cancer cells. See Table 1 for the altered parameters and their definitions.

Table 1. The main parameters defining a virtual patient. Two cancer cell types were included, thus index $i = 1, 2$.

Symbol	Meaning
α_T	Division attempt rate of active killer T-cells.
ξ_i	Rate at which T-cells kill cancer cell subpopulation i.
φ_i	Rate at which cancer cell subpopulation i makes killer T-cells ineffective.
m	Maximum rate of killer T-cell activation.

In addition to parameters, different treatment options were considered for different virtual patients. See Table 2 for the treatment parameters and in which case studies they were considered. We investigated also a few virtual patients without any treatment to monitor the dynamics in an untreated situation.

Table 2. The treatments altered for each case study. Here index $i = 1, 2$.

Symbol	Meaning	Case study
ρ_i	Effect of immunotherapy on cell type i.	1, 2, 3 and 4
β_i	Rate at which cell type i dies due to targeted treatment.	3
c_p	Concentration of the cytostatic drug.	4

We calculated numerically (Runge-Kutta method, RK45) the dynamics of ODEs for each virtual patient. We compared the numerical solutions qualitatively to observed clinical outcomes in cancer [42; 43; 44; 45; 46; 47] to justify the majority of selected parameter values. The virtual patients and their parameter values were selected to

represent different qualitative results, such as progressive, chronic or dormant disease, that have been observed in real patients. Furthermore, the cancer cell doubling times were calculated for each case study and they were found reasonable compared to experimental observations in melanoma [48]. The value of maximum proportion at which cancer cells limit each other's resource consumption (w) was selected so that, multiplied by the saturation of cancer cells, it fell into the limit of 4–56% relative volume of necrotic tissue in melanoma [49]. For the selection of T-cell parameters, we assumed that if the active killer T-cells have existed in the system, a small density remains even if the cancer cell density becomes zero (memory in the immune system).

Generally estimated values have to be used, since in clinical practice it is still impractical or even impossible to estimate all parameters individually. However, based on the additional sensitivity analysis, the most important individual parameters relate to the cancer cell and T-cell interactions (ξ_i and φ_i), the infiltration of T-cells (θ) and the activation of the T-cells (m). Perturbations in these parameter values affected the treatment outcome the most, and for example, the possibility of dormant disease versus inevitable relapse depended on them.

It was assumed that an initial immune response had already occurred, and investigated virtual patients started with densities of 0.05 for all cell types. However, the initial state affects the outcome and required treatment schedule. For example, if the cancer cell density is high with nearly non-existent T-cell density, an intense initial treatment schedule may be required to gain a treatment response.

In the case studies we included one or two cancer cell subpopulations (denoted by 1 and 2). However, more subpopulations could be included along with normally behaving cell types. One cancer cell type is considered to divide faster ($s_{C_1} > s_{C_2}$) and with targeted therapy, one subpopulation is considered resistant ($\beta_1 = 0$) while the other one remains sensitive ($\beta_2 > 0$).

2.3.1   No treatment

We investigated a few baseline cases to gain insights into possible outcomes when treatment is not given. In some cases the treatment was not even needed as the immune system is able to keep cancer in control [50; 51]. Depending on the qualities of the immune system (e.g. the T-cell proliferation and activation rates), the cancer cell density approached a fixed steady state, or the density fluctuated as the T-cells kept defeating the cancer cells at each relapse attempt. However, in practice such behavior is likely to happen in the early stages of cancer development and it is not a guarantee, that cancer would not variate further and relapse.

Some patients are less fortunate, and despite a possible immune response, cancer eventually dominates and potentially becomes fatal. In Figure 4 the T-cell density quickly decreases without treatment, and the cancer cell densities increase. Eventu-

ally, the less aggressive subtype C_2 starts to decrease as C_1 starts to dominate. Carrying capacity and resources start to limit the cancer cell density, however, a smaller cancer density may have already proven fatal to the patient. For such patients, the treatment is needed for a chance of recovery. Different treatment choices may lead to different outcomes and thus it is important to analyze the options. Unfortunately, even with careful planning, the treatment may not always lead to full recovery and relapse is inevitable.
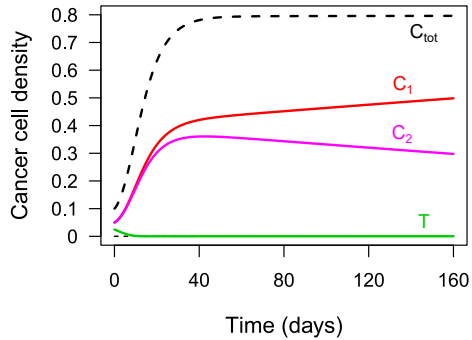
Figure 4. Cancer cell densities for two subtypes (C_1 in red, C_2 in magenta) with the total cancer cell density (C_{tot}, black dashed) and the active killer T-cell density (T, green). (Adopted with permission from Publication I: Fig. 2a.)

2.3.2 Mono-immunotherapy

Immunotherapy has been used in the practice as a monotherapy [52; 46]. We investigated two different virtual patients who received mono-immunotherapy either as a single-shot (case study 1) or with repeated treatment periods (case study 2). For the case study 2, multiple different treatment schedules were considered. For both of these case studies, the virtual patients would suffer from the failure of immune response (see Figure 4).

Single-shot immunotherapy (case study 1)

For the case study 1, we considered one cancer cell subpopulation. We investigated how the attractor landscape changed based on the treatment and how the cancer cell density was affected by this change. The immunotherapy was initiated when the cancer cell density exceeded a pre-defined detection limit threshold (here set to 0.5). As seen in Figure 5a, only one treatment period is enough to revive the T-cell density and the immune system is able to regulate cancer to a dormant state [42; 43; 44; 45]. A single dose of immunotherapy (specifically anti-PD-1) has been observed to cause major responses also in real patients [52; 53].

Here the patient's cancer and immune system characteristics enabled the change in the attractor (full blown cancer versus a dormant cancer). Without treatment, the attractor landscape had two possible steady states. Due to the initial condition, the cell densities started to reach the attractor with high cancer cell density and low killer T-cell density (Fig. 6a top row). The immunotherapy changed the attractor landscape for the duration of treatment period, allowing the cell densities to approach a different steady state (Fig. 6a bottom row). After the treatment, the attractor landscape
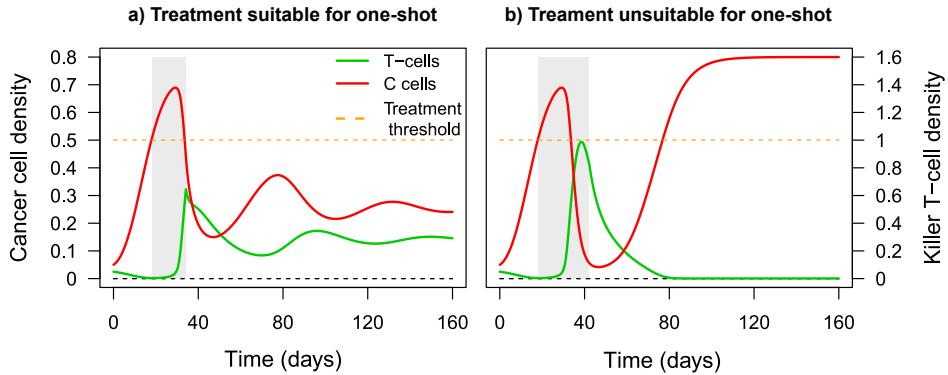
Figure 5. a) The one-shot immunotherapy is given for a period of 16 days (grey bar) and a dormant state is reached. b) The immunotherapy is given for a longer period (24 days). The attractor is the original with high cancer cell density. As the threshold of 0.5 is exceeded again, the treatment would be repeated. (Panel a adopted with permission from Publication I: Fig. 3a.)

reverted back, however, the cell densities had changed and a different steady state was reached as the original attractor had now become unattainable (Fig. 6a top row). Thus, depending on the patient's biological qualities, there may exist a manageable dormant state, even if originally cancer is rapidly increasing. However, the timing and dosage of the single-shot immunotherapy were crucial to achieve the change from the original, unfavorable attractor to the manageable dormant state. With an unfavorable treatment (e.g. too short or too long duration) cancer would have prevailed after a small decrease in the cancer cell density (see Fig. 5b and Fig. 6b).

Repeated immunotherapy (case study 2)

Despite the success of one-shot immunotherapy in some cases, many cases require repetitive treatment. For example, in practice nivolumab and pembrolizumab (immune-checkpoint inhibitors) are administered every 2nd or 3rd week respectively. We investigated a virtual patient with two cancer cell subpopulations (C_1 and C_2) with one slightly more aggressive than the other ($s_{C_1} = 1$, $s_{C_2} = 0.95$). The virtual patient would suffer from a rapid increase in the cancer density if no treatment is used (Fig. 4 is for this patient).

   First we investigated how different treatment initiation options affected the outcome, and whether there was a superior scheduling technique. We compared a pre-set treatment periods to threshold-based treatment initiation. Pre-set treatment periods are widely used option, however, a more adaptive alternative is to initiate the treatment when a total cancer cell count (i.e., total tumor burden) exceeds a threshold. We investigated the options by changing the treatment period and, depending on the scheduling, either interval between treatments (drug holiday) or the given threshold.
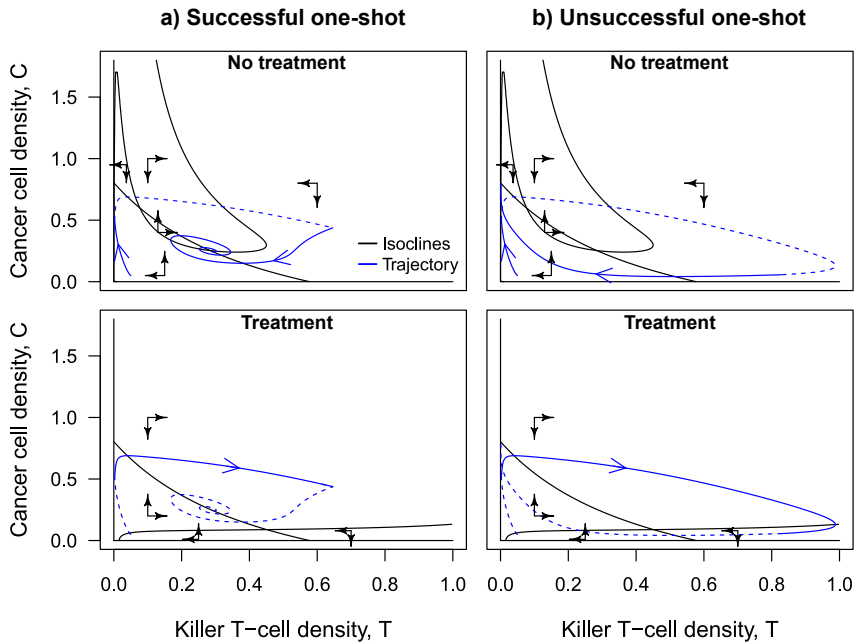
Figure 6. Phase plane plots showing the isoclines (black lines) of the killer T-cell density T and cancer cell density C, a) for a successful one-shot immunotherapy and b) for an unsuccessful one-shot immunotherapy. The trajectories with respect to time are shown in blue. The line is solid when the treatment status corresponds to the phase plane plot (top row: during no treatment, bottom row: during treatment). The treatment period is a) 16 days or b) 24 days.

As expected, for the pre-set periods, short treatment periods required short drug holidays. If the drug holiday was continued for too long, the treatment might fail even if the treatment was repeated. Interestingly, for the threshold-based initiation, the treatment period length had little effect on the outcome (total cancer cell mean density) since short treatment periods were repeated depending on the cancer density at the end of the previous treatment. If the threshold was still exceeded, the treatment was repeated immediately without a drug holiday. However, the selection of threshold affected the outcome, as for the higher thresholds the cancer cell density reached a higher level before the treatment.

Both of the options had treatment regimen parameters that resulted in small cancer mean density (examples in Fig. 7). Choosing a specific treatment period along with either a suitable drug holiday or a threshold might result in a better therapeutic effect. However, a small cancer mean density did not necessarily imply a good treatment, as it might require long treatment periods with short or non-existent drug holidays. Such heavy treatment scheduling might be unbearable for the patient and thus it is important to consider also the time spent under treatment. If the treatment period and drug holiday were selected carefully, successful treatment result could be reached without increasing the time in treatment in the chosen time interval (Fig. 7).
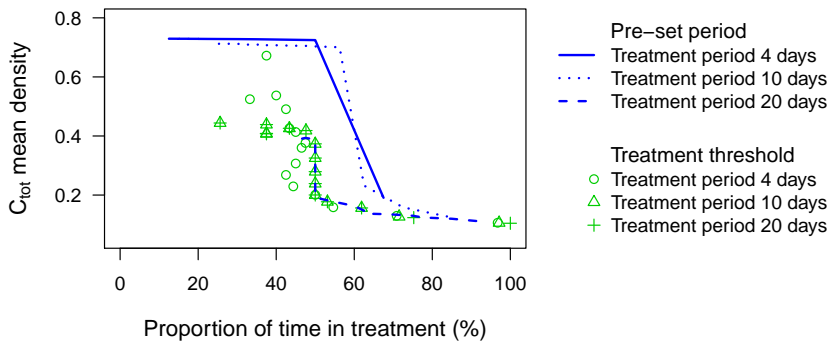
Figure 7. Mean cancer cell density with respect to the proportion of time in treatment (% from the total follow-up time interval). Either pre-set periods (blue) or threshold-based initiation (green) is used with treatment periods of 4, 10 or 20 days. For the pre-set periods, the proportion of time in treatment changes when the drug holiday is changed. For the threshold-based treatment initiation, the threshold level determines the time in treatment. (Adopted with permission from Publication I: Fig. 5.)

Overall, cancer was kept in control more likely with a threshold-based treatment initiation, since the treatment was repeated without drug holiday for as long as needed to decrease the total cancer density. Despite the possibility of a long continuous treatment period, the sufficient decrease in cancer density might have led to a longer drug holiday before the density reached the given threshold again. In practice, however, the use of pre-set treatment periods is more applicable since the threshold-based initiation requires heavy monitoring of the cancer cell density, and this would require improvement in the diagnostic tests.

Adapting the treatment (case study 2)

To make the approach of pre-set periods more adaptive and reduce the time in treatment (less side effect and costs) without losing the treatment success, we changed the treatment schedule in the middle of the follow-up period. Since a long drug holiday would lead to almost immediate treatment failure, the treatment was started with a tighter schedule (treatment 12 days, drug holiday 6 days). After the third treatment period, the drug holiday was increased (16 days). Compared to the non-adaptive scheduling, the successful adapted treatment resulted in a similar total cancer cell mean density while the time in treatment decreased (Fig. 8). Despite the successful treatment adaptation in this case, the treatment outcome was sensitive for the selection of the new schedule. If the drug holiday was increased even more (to 20 days) there was a notable increase in total cancer cell density, since the T-cell density would decrease on an unrecoverable level during the drug holidays. Adapting the time of the schedule change would not have helped, if the new drug holiday was too long.
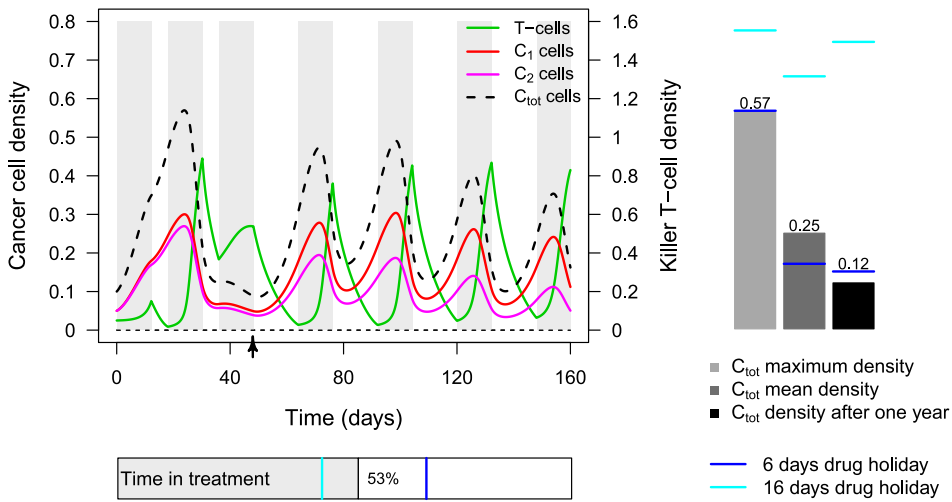
Figure 8. The pre-set treatment period of 12 days, followed by 6 days of drug holiday, is changed to schedule with 16 days of drug holiday after 48 days (black arrow). Right-side barplots: the treatment success measures, with corresponding values for non-adaptive treatments with 6 days of drug holiday (blue) and 16 days of drug holiday (cyan). Bottom bar: proportion of time spend in treatment. (Adopted with permission from Publication I: Fig. 6a.)

2.3.3   Combination therapy

In practice, immunotherapy is also used in a combination with other treatments [54]. We investigated especially combinations with targeted treatment or chemotherapy. We compared the effectiveness of combination treatments against monotherapies.

Immunotherapy with targeted treatment (case study 3)

The targeted treatment targets a specific molecular aberration in a cancer cell. Unfortunately, some cancer cells may be missing the aberration making them treatment resistant against that treatment. With the virtual patient in case study 3, we investigated a situation with two cancer cell subtypes and assumed that only one of the subtypes is sensitive (here C_2) whereas the other is resistant (C_1). We tested multiple different treatment strategies by simultaneous threshold-based treatment initiation, and altering the durations of targeted and immunotherapy. The combined treatment duration was set to a constant of 14 days, for simplicity.

Some duration combinations (e.g. both with 7 day duration), resulted in a chronic disease with repeated treatments. Eventually the sensitive subpopulation diminished due to the targeted treatment and the resistant subpopulation prevailed. After this, the targeted treatment became useless and the immunotherapy was the main effective treatment. On the other hand, a stable disease was also reached with selected combinations.

We calculated the total cancer cell mean density and number of treatment initiations for varied treatment thresholds and proportions of targeted treatment (Fig. 9). As expected, smaller thresholds led to smaller cancer mean densities with multiple treatment initiations. However, if the stable disease was reached, the number of treatment initiations stayed low while the cancer mean density was still relatively low. Such a stable disease was reached with mono-immunotherapy (0% of targeted treatment), but also with carefully selected monotherapy of targeted treatment (100% of targeted treatment). However, in general, the combination therapy worked better than targeted therapy alone since after the sensitive subpopulation had disappeared, the targeted treatment had no effect.
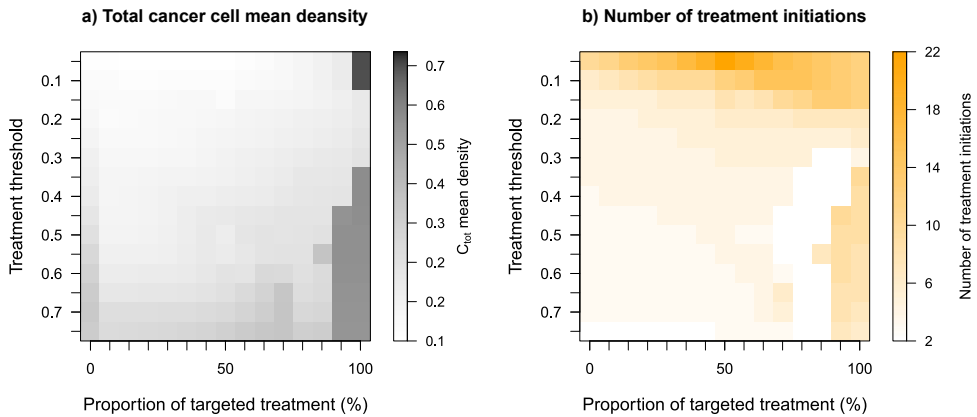
Figure 9. The effect of immunotherapy and targeted treatment combinations. a) The total cancer cell mean density with respect to treatment threshold and the proportion of targeted treatment (here 0% equals 14 days of immunotherapy, 100% equals 14 days of targeted therapy, 50% equals 7 days of both initiated simultaneously). b) The corresponding numbers of treatment initiations. (Adopted with permission from Publication I: Fig. 7d and e.)

In Publication I we considered only a case where the two cancer subpopulations had proliferation rates close to each other (1 vs. 0.95) and the less aggressive subpopulation was sensitive to the targeted treatment. If the difference between the proliferation rates is higher (1 vs. 0.65) and the more aggressive subpopulation is sensitive, there is another way to manage cancer with targeted therapy alone. Assuming that there is no other targeted treatment to target the resistant subpopulation, the resistant subpopulation could theoretically be controlled by the dominating, more aggressive subpopulation. Then the sensitive subpopulation would be kept under control by the targeted treatment. Figure 10 presents a case where the more rapidly dividing subpopulation C_1 is sensitive and the subpopulation C_2 is resistant. The treatment is initiated when the C_1 cell density exceeds a given threshold. The resistant subpopulation is controlled by the sensitive subpopulation and T-cell increase during treatments (caused by increase of cancer cell death and antigen delivery). However,

17

despite cancer being under control, this method would require monitoring the densities of specific subtypes instead of total cancer cell density, and thus the application in practice may be challenging.
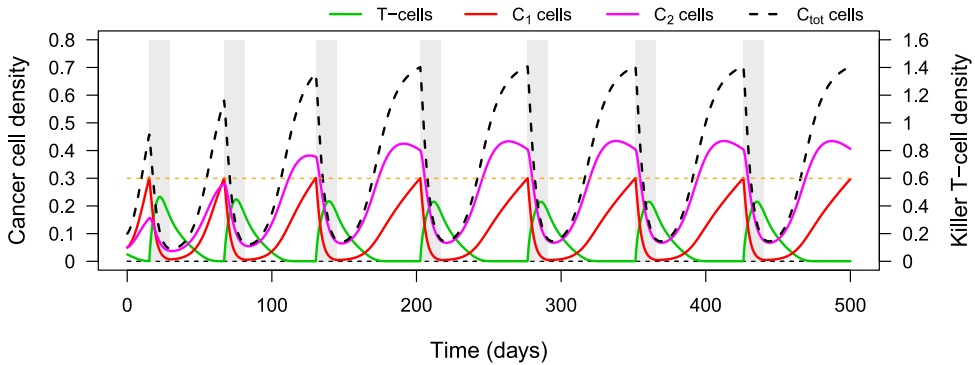
Figure 10. The dynamics in a case, where the treatment-sensitive subpopulation C_1 is notably less aggressive than the treatment-resistant subpopulation C_2. Targeted treatment is initiated when the density of the sensitive population exceeds the treatment threshold.

Immunotherapy with chemotherapy (case study 4)

For the case study 4, we considered a virtual patient who received chemotherapy either alone or in combination with immunotherapy. To minimize the side effects, it would be preferred to use the minimal effective treatment regimen (small dosages, short treatment periods). Depending on the treatment choices, cancer was chronic with repetitive treatment or, more rarely, a stable disease was reached with one or two treatment periods. We observed that a combination treatment often resulted in shorter time in treatment when compared to the chemotherapy alone. Simultaneously, there was a possibility of smaller cancer cell mean density. The side effects were calculated as the proportion of T-cell loss caused by cytostatic drug to the overall T-cell loss. For short treatment periods, the combination therapy decreased the side effects when compared to the chemotherapy. For longer treatment periods, the situation shifted slightly to the opposite case, because the side effects were calculated as a proportion and the extended immunotherapy decreased the overall loss of T-cells. However, the differences were mild and other types of side effects and tolerability issues could affect the comparison of chemotherapy and combination treatment.

3 Cancer metapopulation model with angiogenesis

In Publication II, cancer was modelled as a metapopulation, in which cancer population patches along with the dispersal pool (here the circulatory system) form a metapopulation. Cancer cells may inhibit patches, which are possible sites for clusters of cancer cells. Cells may emigrate into the dispersal pool and immigrate from there into patches (Fig. 11). Cancel cells have an emigration strategy, which tells how eagerly the cell tries to emigrate and leave the patch. We included angiogenesis, which is the formation of new vessels. Cancer cells may contribute to the angiogenesis trying to enhance the resource (e.g. glucose) availability. The elevated resource inflow eases the cell growth when the tumor grows and the pre-existing vasculature becomes insufficient. Anti-angiogenic treatment is designed to prevent the angiogenesis and thus to inhibit the cancer cell growth. In addition to angiogenesis mechanism in our metapopulation model, we also included an anti-angiogenic treatment.
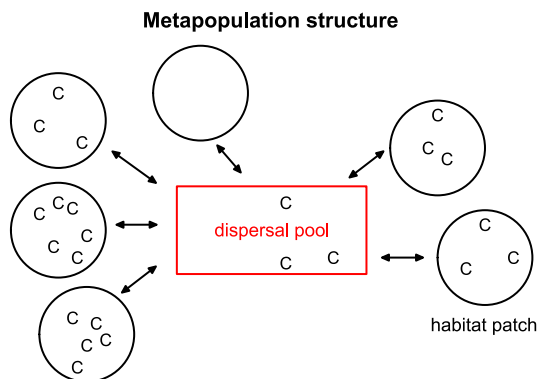
Figure 11. The metapopulation structure with cancer cells (C) inhabiting the habitat patches, i.e., possible sites for cluster of cells (black circles). Cell may emigrate into the dispersal pool, i.e., the circulatory system (red rectangle) and immigrate from there into habitat patches. (Adopted with permission from Publication II: Fig. 1.)

3.1 Literature review

As mentioned in Chapter 2, cancer has been widely modelled with different approaches. However, to our knowledge, our model in Publication II is the only one considering the cancer ecosystem as a continuous-time metapopulation with varying strategies. The metapopulation modelling approach has been previously used to investigate population dynamics in various other scenarios, that are not cancer specific (see e.g. [55; 56; 57; 58; 59; 60; 61; 62]). The metapopulation dynamics along with strategy evolution can be investigated using tools of adaptive dynamics [63; 64; 65].

Angiogenesis is the formation process of new blood vessels from pre-existing vasculature. It is an important step in the cancer development, since the expanding tumor requires new blood supply to maintain growth [66; 67; 68]. The cancer cells develop signalling mechanisms, such as secreting VEGF (vascular endothelial growth factor), that stimulate angiogenesis [69]. These mechanisms may be targeted by anti-angiogenic treatments that prevent the angiogenesis (e.g., anti-VEGF) [33; 34; 35]. However, as with many cancer treatments, cancer cells may develop treatment resistance to anti-angiogenic treatment [70; 33]. For example, the targeted angiogenesis mechanism might be bypassed with another signalling pathway (e.g., fibroblast growth factors [33]).

3.1.1 Angiogenesis modelling

Angiogenesis has been modelled before in relation to cancer (see e.g. [11; 12; 13; 71; 72; 73]), and also in other contexts, such as wound-healing [74; 75]. For example, Letellier et al. [11], Pinho et al. [12] and Yonucu et al. [13] modelled cancer with ODEs for different cell types (e.g. cancer, normal/host) and vasculature. Angiogenesis mechanism was included through changes in the endothelial cells or blood vessel distribution. Nagy and Armbruster [71] considered differential equations for tumor mass, immature vascular endothelial cell mass and total microvessel length. They also included cells' energy status in form of ODEs for adenosine 5' mono-, di- and triphosphatases (AMP, ADP and ATP) to investigate the trade-offs between proliferation and angiogenesis contribution.

In our model in Publication II, we have included angiogenesis through changes in resource inflow instead of including an additional cell type. The resources (e.g. glucose or oxygen) flow into and out of the tumor microenvironment and higher angiogenesis contribution by the cells elevates the resource inflow, which further aids the cell proliferation. However, secreting angiogenic factors (like VEGF) requires energy, and we included a trade-off between birth rate and angiogenesis contribution. In our model, angiogenesis was also considered to increase the emigration rate

through increased vasculature [76]. However, there have been mixed results on the relation of angiogenesis and emigration, since cancer angiogenesis usually leads to distorted veins, through which the access is compromised [77].

3.1.2 Treatment modelling

When modelling cancer angiogenesis, an anti-angiogenic treatment could be included to counter the effects. For example, Pinho et al. [12] and Yonucu et al. [13] modelled the anti-angiogenic treatment with ODEs for therapy agents. The treatment concentration then affected the amount of endothelial cells or vessels. In our metapopulation model, the effect of anti-angiogenic treatment directly cancels the effects of angiogenesis within the resource flow and the emigration rate. Since the original (mature) vessels are assumed to be VEGF independent [78; 79], a baseline resource inflow will remain even with high levels of anti-angiogenic treatment.

Thus, an anti-angiogenic treatment as a monotherapy does not typically lead to a full response and a complete eradication requires a combination treatment [17; 80; 81]. Pinho et al. [12] and Yonucu et al. [13] included chemotherapy along with anti-angiogenic therapy. Also other treatment options, like immunotherapy could be considered for a combination with anti-angiogenic treatment [82; 83]. Instead of regarding another treatment as an adjuvant therapy for the anti-angiogenic treatment, the situation could be considered other way around. Anti-angiogenic treatments could be considered to reduce the need for more toxic treatments, since anti-angiogenic treatments generally have manageable side effects (e.g., hypertension [34]), while treatments like chemotherapy may have severe side effects. However, despite being generally well tolerated, the anti-angiogenic treatment may also lead to increased risk of bleeding complications and gastrointestinal perforation [84; 85]. In our model, we included a cytotoxic treatment to investigate how the combination affected the outcome compared to monotherapies.

A combination treatment may be required also since the cancer cells may develop resistance to the anti-angiogenic treatment [70; 33]. We considered only a single angiogenesis mechanisms (like VEGF secretion), but other proangiogenic factors like fibroblast growth factors (FGFs) and platelet derived growth factors (PDGFs) [33] could be used to promote angiogenesis. We included the resistance to anti-angiogenic treatment by preventing the treatment effect on resistant cells.

3.2 Model

We constructed a metapopulation model for cancer with habitat patches and dispersal pool (see Fig. 11). The state and living conditions in a patch are determined by the resource inflow through vasculature and the cells living in the patch. The patches have no direct interactions, and the cells immigrate only through the dispersal pool

(circulatory system). We omitted the spatial relation of patches and the distance is not considered in the immigration of cells. However, the population size of the new patch candidate affects the immigration probability, since the cells are more likely to immigrate into a less-populated patch.

3.2.1 Within-patch dynamics

Dynamics within a patch depend on the resource availability and the cancer cells. The resource dynamics are assumed to be fast compared to the cancer cell dynamics.

Resources

As in the Publication I, we included the resources in our metapopulation model in Publication II. Resources (R) (e.g. glucose) follow the chemostat dynamics [36] when flowing into and out of the patch. The constant baseline inflow $\hat{R}$ was included with possibility of angiogenesis-based increase. Angiogenesis-contributing cells enhance the vasculature, and the resource inflow by the factor

$$f(\boldsymbol{n}, \boldsymbol{a}) = \left(1 + \frac{A_{\max} \sum_{i=1}^{k} n_i a_i}{1 + \sum_{i=1}^{k} n_i a_i} \right), \tag{7}$$

where $A_{\max}$ is the upper bound, based on the limited space for the new vessels. Vectors $\boldsymbol{n} = (n_1, ..., n_k)$ and $\boldsymbol{a} = (a_1, ..., a_k)$, where n_i is the number of type i cells and a_i is the corresponding angiogenesis strategy (i.e., how much a type i cell contributes to angiogenesis). Cells collect resources by law of mass action with their resource consumption rate s_i [37]. Thus, including the outflow concentration R and the relative flow speed λ, local resources follow the following differential equation:

$$\frac{dR}{dt} = \lambda \left(f(\boldsymbol{n}, \boldsymbol{a}) \hat{R} - R \right) - R \sum_{i=1}^{k} n_i s_i. \tag{8}$$

However, if the anti-angiogenic treatment is administrated, it prevents the angiogenesis and the increase in resource concentration. Cancer cells may develop resistance ρ_i to anti-angiogenic treatment [70; 33]. Resistant cells ($0 < \rho_i \leq 1$) decrease the effect of anti-angiogenic treatment on their angiogenesis contribution. Modified Equation (7) includes the anti-angiogenic treatment ψ_a and the treatment resistance ρ_i:

$$f(\boldsymbol{n}, \boldsymbol{a}, \boldsymbol{\rho}, \psi_a) = \left(1 + h(\psi_a) \frac{A_{\max} \sum_{i=1}^{k} n_i a_i l(\rho_i, \psi_a)}{1 + \sum_{i=1}^{k} n_i a_i} \right), \tag{9}$$

where $\rho = (\rho_1, ..., \rho_k)$ are the resistance strategies of cell types $1, ..., k$. The treatment effect is

$$h(\psi_a) = \frac{1}{1 + \psi_a}, \tag{10}$$

where ψ_a is the concentration of anti-angiogenic treatment. The resistance effect

$$l(\rho_i, \psi_a) = 1 + \psi_a \rho_i \tag{11}$$

is determined by the treatment function $h(\psi_a)$ and cancels the treatment effect only on cell type i. Thus, if the cell type i is resistant and the cell type j is sensitive, only the contribution of type i transpires. It is assumed that the resource dynamics are fast, and in the equilibrium ($dR/dt = 0$) the resource concentration is

$$R^*(\boldsymbol{n}, \boldsymbol{a}) = \frac{\lambda f(\boldsymbol{n}, \boldsymbol{a}) \hat{R}}{\lambda + \sum_{i=1}^{k} n_i s_i}. \tag{12}$$

Cancer cells

The within-patch cancer cell dynamics were modelled as a continuous-time Markov chain (see Fig. 12 for a monomorphic population), in which the population's state is determined by the numbers of cell types and the state changes based on the cell proliferation, death and migration. It was assumed that a patch could have a maximum of K cells and no division would happen in a full patch.
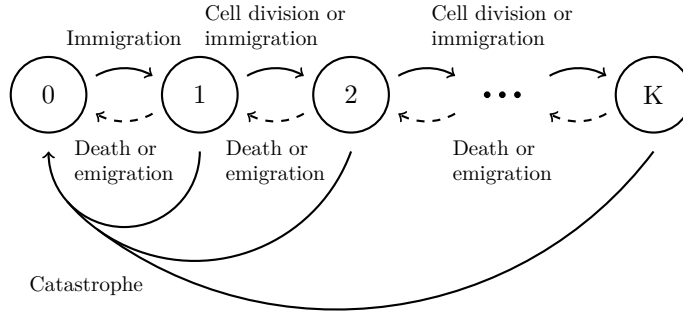
Figure 12. The states and transitions of the Markov chain describing monomorphic (i.e., all cells are of the same type) resident population dynamics. (Adopted with permission from Publication II: Fig. 2.)

Cells collect resources and proliferate based on the resource intake, thus the birth rate of cell type i is

$$b_{\boldsymbol{n},\boldsymbol{a},i} = \gamma s_i R^*(\boldsymbol{n}, \boldsymbol{a}) g(a_i, \rho_i), \tag{13}$$

where R^* is the resource concentration in equilibrium, s_i is the resource consumption rate and γ is the conversion coefficient from resource intake to cell division. Since angiogenesis contribution reserves resources from proliferation, the trade-off

$g(a_i, \rho_i)$ was included. In addition, it was assumed that acquiring and maintaining resistance ($\rho_i > 0$) requires energy and has a trade-off on proliferation. The trade-off is

$$g(a_i, \rho_i) = \frac{1}{1 + a_i + \beta\rho_i}, \tag{14}$$

where, β is the trade-off factor for resistance. The trade-off factor of angiogenesis was set to 1.

The cells die with the rate

$$d_{n_T} = d_0 + \delta n_T + \psi_c, \tag{15}$$

where d_0 is the baseline death rate, ψ_c is the effect of cytotoxic treatment and $n_T = \sum_{i=1}^{k} n_i$ is the total number of cells in the patch. The factor $\delta = 1/K$ is positive, as it was assumed that a higher population size leads to a higher death rate [86]. Cells emigrate with the rate

$$q_{\boldsymbol{n},\boldsymbol{a},e_i} = e_i f\left(\boldsymbol{n}, \boldsymbol{a}\right), \tag{16}$$

where e_i is the emigration strategy (i.e., how easily cell leaves the patch). The factor f is as in Equation (9) since it was assumed that the changes in vasculature affect the emigration probability [76; 87; 88].

3.2.2 Metapopulation dynamics

The state of a patch depends on the numbers of cells in the patch. A metapopulation's state is investigated by calculating the distribution of the cell numbers. In a monomorphic population the probabilities p_n, i.e., the probabilities that a randomly chosen patch has n cells, satisfy the differential equations (forward Kolmogorov equations):

$$\frac{dp_0(t)}{dt} = -\alpha D S_0 p_0(t) + [d_1 + q_{1,a,e}]\, p_1(t) + \mu \sum_{n=1}^{K} p_n(t)$$

$$\frac{dp_n(t)}{dt} = - \left[\alpha D S_n + n(b_{n,a} + d_n + q_{n,a,e}) + \mu\right] p_n(t)$$
$$+ \left[\alpha D S_{n-1} + (n-1)b_{n-1,a}\right] p_{n-1}(t) + (n+1)\left[d_{n+1} + q_{n+1,a,e}\right] p_{n+1}(t)$$

$$\frac{dp_K(t)}{dt} = - \left[K(d_K + q_{K,a,e}) + \mu\right] p_K(t) + \left[\alpha D S_{K-1} + (K-1)b_{K-1,a}\right] p_{K-1}(t), \tag{17}$$

where the dispersal pool size D satisfies the differential equation:

$$\frac{dD(t)}{dt} = - \left(\alpha \sum_{n=0}^{K} p_n(t) S_n + \nu \right) D(t) + \sum_{n=1}^{K} q_{n,a,e} n p_n(t). \tag{18}$$

Here ν is the death rate of cancer cells in the dispersal pool. Cells encounter patches with the rate α and immigrate with the probability $S_n = (K-n)/K$ upon encounter. Thus, the cells are more likely to immigrate into less inhabited patches.

In a metapopulation-dynamical steady state $\frac{dp_n(t)}{dt} = 0$ and $\frac{dD(t)}{dt} = 0$. However, since $p_n(t)$ are probabilities, they must satisfy $\sum_{n=0}^{K} p_n(t) = 1$, and thus one equation in (17) needs to be replaced by $p_0(t) + p_1(t) + \cdots + p_K(t) = 1$. In a steady state, $p_n(t)$ and $D(t)$ do not depend on time, so that $p_n(t) = \bar{p}_n$ and $D(t) = \bar{D}$. From the linear system of equations

$$
\begin{aligned}
0 &= -\alpha D S_0 \bar{p}_0 + [d_1 + q_{1,a,e}] \bar{p}_1 + \mu(1 - \bar{p}_0) \\
0 &= -[\alpha D S_n + n(b_{n,a} + d_n + q_{n,a,e}) + \mu] \bar{p}_n \\
&\quad + [\alpha D S_{n-1} + (n-1)b_{n-1,a}] \bar{p}_{n-1} + (n+1)[d_{n+1} + q_{n+1,a,e}] \bar{p}_{n+1} \\
1 &= \bar{p}_0 + \bar{p}_1 + \cdots + \bar{p}_K.
\end{aligned}
\tag{19}
$$

The probabilities $\bar{p}_n$ can be solved for a fixed value of D. Based on Equation (18) the equilibrium value $\bar{D}$ must then satisfy

$$
1 = \frac{\sum\limits_{n=1}^{K} q_{n,a,e} n \bar{p}_n(\bar{D})}{\left(\alpha \sum\limits_{n=0}^{K} \bar{p}_n(\bar{D}) S_n + \nu \right) \bar{D}},
\tag{20}
$$

where $\bar{p}_n(D)$ denote the solution of (19). Solutions $\bar{p}_n$ and $\bar{D}$ were searched numerically.

3.2.3 Evolutionary dynamics

Cell's strategies variate randomly, forming new variant cells that then experience the environment set by the resident population. The variant's invasion fitness is the long-term exponential growth rate in this environment [89]. Only a variant with a positive invasion fitness may invade and become a new resident. However, calculating the invasion fitness is often complicated and, instead, the metapopulation fitness R_{metapop} [90; 59; 58] is calculated to determine the sign of the invasion fitness.

From an initially small variant population in the dispersal pool, a focal variant may immigrate into a patch. The variant and all of its descendants form a variant colony in the patch and, due to the variants rarity, no other variants are expected to arrive during the lifetime of the variant colony. The variant colony sends emigrants to the dispersal pool and the variant's metapopulation fitness is the expected number of variant emigrants produced by the variant colony during its lifetime (i.e. the time before the variant colony goes extinct).

The state of the variant colony is determined by the number of variants n_m and residents n_r, which change according to a Markov chain. When the focal variant immigrates, there is exactly one variant ($n_m = 1$). The number of residents depends on chance, based on the resident population distribution (p_n). The initial probability distribution of the Markov chain is

$$
\begin{aligned}
\delta_0(n_r, 1) &= \frac{p_{n_r} S_{n_r}}{\sum_{n=0}^{K-1} p_n S_n}, & \text{for } 0 \leqslant n_r < K \\
\delta_0(n_r, n_m) &= 0, & \text{for } n_m > 1.
\end{aligned}
\tag{21}
$$

The transition intensities from the state (n_r, n_m) to neighboring states are

$$
\begin{aligned}
c_{n_r,n_m}^{0,+} &= n_m b_{\boldsymbol{n},\boldsymbol{a},m}, & \text{if } n_T = n_r + n_m < K \\
c_{n_r,n_m}^{0,-} &= n_m(d_{n_T} + q_{\boldsymbol{n},\boldsymbol{a},m}) \\
c_{n_r,n_m}^{+,0} &= \alpha D S_{n_T} + n_r b_{\boldsymbol{n},\boldsymbol{a},r}, & \text{if } n_T = n_r + n_m < K \\
c_{n_r,n_m}^{-,0} &= n_r(d_{n_T} + q_{\boldsymbol{n},\boldsymbol{a},r}).
\end{aligned}
\tag{22}
$$

The subscript denotes the original state and the superscript indicates the change in corresponding numbers of individuals. The transition intensity out of the state (n_r, n_m) is

$$
c_{n_r,n_m} = c_{n_r,n_m}^{0,+} + c_{n_r,n_m}^{0,-} + c_{n_r,n_m}^{+,0} + c_{n_r,n_m}^{-,0} + \mu,
\tag{23}
$$

where μ is the rate of catastrophes, which erase the local population entirely (e.g. surgery). When a transition happens, the probability that the population changes from the state (n_r, n_m) to the state $(n_r, n_m + 1)$ is $c_{n_r,n_m}^{0,+}/c_{n_r,n_m}$. Other transition probabilities are formed correspondingly and they are collected to the transition probability matrix P.

The expected number of visits w in each state are calculated from [91]:

$$
w = \delta_0(I - P)^{-1},
\tag{24}
$$

where I is the identity matrix and the matrix inverse exists for transient states. The fitness is calculated from

$$
R_{\text{metapop}} = \frac{\alpha_m \sum_{n=0}^{K-1} p_n S_n}{\nu + \alpha_m \sum_{n=0}^{K-1} p_n S_n} \sum \frac{n_m q_m w_{n_r,n_m}}{c_{n_r,n_m}},
\tag{25}
$$

where q_m is the emigration rate of variants and w_{n_r,n_m} corresponds to the state (n_r, n_m) in the vector w. The invasion fitness is positive if and only if $R_{\text{metapop}} > 1$.

Evolutionary dynamics are illustrated using pairwise invasibility plots (PIPs), in which variant's fitness is marked either negative or positive ($R_{\text{metapop}} < 1$ or $R_{\text{metapop}} > 1$ correspondingly) with respect to resident's and variant's strategies. Curves on which $R_{\text{metapop}} = 1$, are called neutral contours. For example, on the

diagonal resident's and variant's strategies are equal and thus the fitness is neutral.

To investigate where the strategy (or strategies) would evolve, a variant's fitness gradient is calculated since a variant's fitness increases the most in the direction given by the fitness gradient. In reality, the strategies do not evolve straight along the gradient, however, in that direction the invasion probability is higher and over time the strategies will evolve to the gradient's direction. For a multi-dimensional strategy (strategy vector) the fitness gradient is

$$
D(a_r, e_r, \rho_r) =
$$

$$
\left. \left(\frac{\partial}{\partial a_m} R_{\text{metapop}}, \frac{\partial}{\partial e_m} R_{\text{metapop}}, \frac{\partial}{\partial \rho_m} R_{\text{metapop}} \right) \right|_{a_m = a_r, e_m = e_r, \rho_m = \rho_r} .
$$

(26)

In case of a one-dimensional strategy, the fitness function (25) is differentiated only with respect to that strategy, after which the variant's strategy is set to be equal to resident's strategy. A point where all the components of the fitness gradient become zero is called evolutionarily singular strategy (or just singular strategy). In a PIP, the singular strategies are positioned at the intersections of the diagonal and other neutral contours. A singular strategy is uninvadable (evolutionarily stable) if there is no strategy that could make an invasion. The opposite holds for invadable singular strategy. A singular strategy is attracting, if near the point smaller values have a positive gradient and higher values have a negative gradient. If the opposite holds, the singular strategy is repelling.

In addition to analyzing the singular strategies, we also monitored their effect on the population level by calculating the average population size $\sum_{n=0}^{K} n p_n$ and the average emigration $\sum_{n=0}^{K} p_n e f(n, a)$.

3.3   Results

In the main analyses, we focused on the strategies (angiogenesis, emigration and resistance) and the treatment parameters' effect on them. First, we investigated the three strategies (angiogenesis, emigration and resistance) separately, while keeping the remaining two as constants. Joint evolution of angiogenesis and emigration strategies was analyzed with anti-angiogenic and cytotoxic monotherapies and with the combination therapy. Finally, the joint evolution of all three strategies was investigated under anti-angiogenic treatment.

Parameter values were selected so that the metapopulation was viable. The selected parameter values were further justified by comparing the observed angiogenesis dynamics qualitatively to real-life observations [17; 66; 80; 67; 81]. The treatment parameters were increased from zero (no treatment) until the population became nonviable, the angiogenesis strategy became zero or the main trend was detected. Other

parameters were mainly kept constant, however, additional analyses were conducted also on their changes and effects on the strategy dynamics (Publication II Supplementary Material). It was noted, that especially the joint dynamics of all three strategies were sensitive to the changes in parameter values, indicating the importance of patient-specific biology and need for personalized treatments.

3.3.1 Single strategies

Angiogenesis increased the birth rate indirectly through resources, however, there was also the direct cost on the birth rate. The relation between benefit (resources) and costs (trade-off) determined whether a positive singular strategy existed (Fig. 13a). Despite the cost for an investing cell, the resource increase benefited the whole patch, including the cell's kin. Therefore, kin selection [92] also played a role in the angiogenesis evolution. If the singular angiogenesis strategy was detected, it was attracting and uninvadable. However, the attracting singular strategy did not necessarily maximize the average population size because the best for individual might differ from the best for the population. In the case anti-angiogenic treatment was added, the angiogenesis strategy would decrease (Fig. 13b), eventually becoming zero if the treatment was high enough.

Emigration evolution was also affected by the kin selection, since by emigrating, the cells left more resources for their relatives (and other cells) in the original patch. The emigrating cells might also directly benefit from the emigration, if the new patch was better than the original. Thus, a positive singular emigration strategy was detected (Fig. 13c). The existence of a positive singular strategy was also reasonable, because the positive catastrophe rate would cause non-viability if the emigration strategy was close to zero (narrow black bars in Figs. 13c and d). Similarly to angiogenesis, the singular emigration strategy did not necessarily maximize the average population size. Addition of anti-angiogenic treatment increased the singular emigration strategy 13d).

Without treatment, the treatment resistance had only a negative effect on proliferation and the strategy evolved to zero (Fig. 13e). With treatment, the situation shifted and a positive singular strategy might exist (Fig. 13f), however, this depended on the level of treatment. We mainly analyzed the resistance strategy together with angiogenesis and emigration strategies (see Section 3.3.3).

3.3.2 Joint evolution of angiogenesis and emigration strategies

We investigated the joint evolution of angiogenesis and emigration strategies, i.e. the both were allowed to variate while the resistance strategy was kept zero. We observed that increasing one strategy component made the other one less favorable
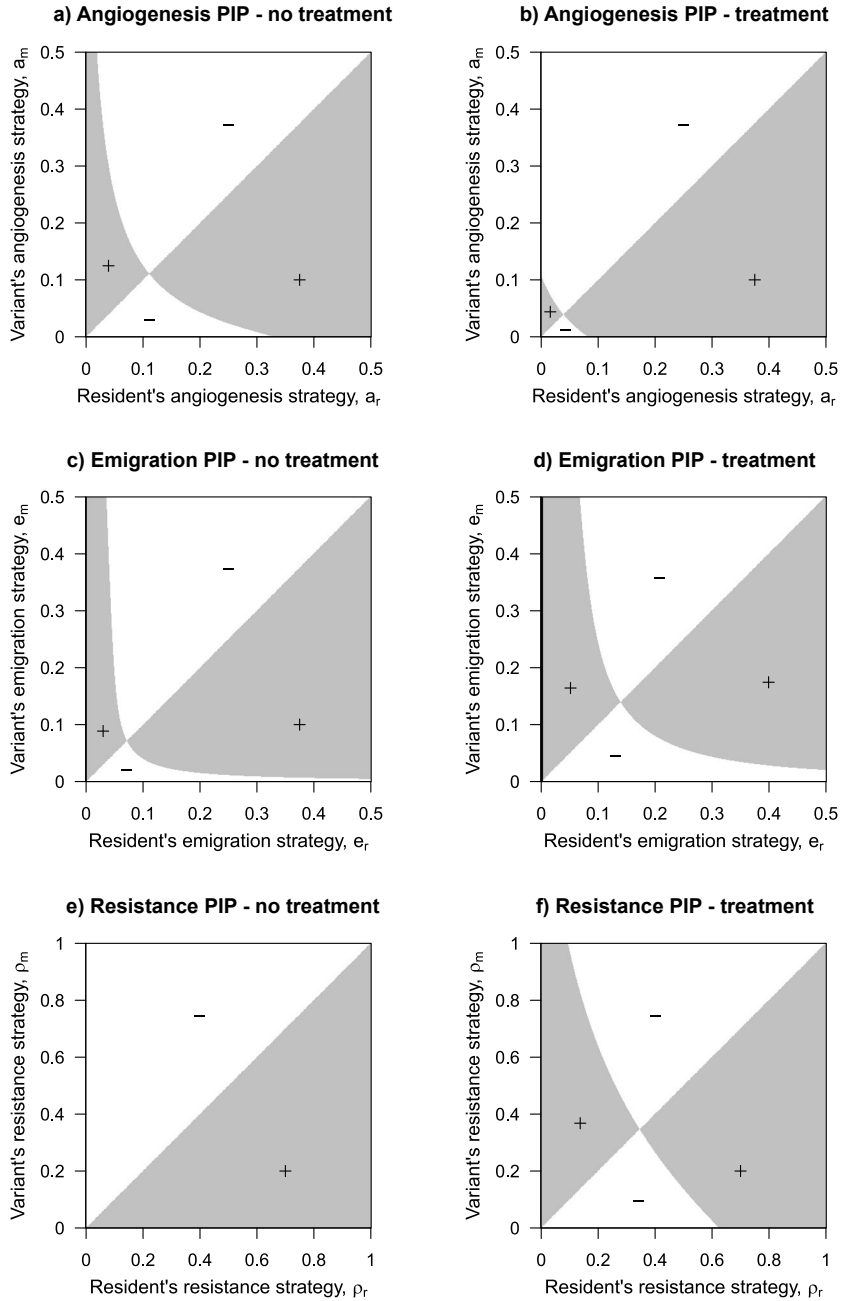
Figure 13. Pairwise invasibility plots (PIP) for a) angiogenesis strategy without treatment and b) with anti-angiogenic treatment. c) PIP for emigration strategy without treatment and d) with anti-angiogenic treatment. e) and f) corresponding PIPs for resistance strategy. In each, the other strategies are kept constant $e = 0.2$, $a = 0.2$ and $\rho = 0$. The anti-angiogenic treatment $\psi_a = 0$ for left panel and $\psi_a = 7$ for the right panel.

for the cancer cells. The joint singular strategy was numerically calculated from the condition $D(a_r, e_r) = (0, 0)$. The singular strategy did not necessarily maximize the average population size, as was observed in the case of a single strategy. Since the parameters defined the conditions for the strategy dynamics, we investigated the parameters' effect on the singular strategies. Especially we focused on the treatment parameters.

Monotherapies

As the anti-angiogenic treatment decreased the benefits of angiogenesis, an increase in the treatment caused the singular angiogenesis strategy to decrease. Consequently, the emigration was compromised and initially the average emigration rate decreased. However, the singular emigration strategy increased with the anti-angiogenic treatment and the decrease in the average emigration rate abated. The singular angiogenesis strategy became zero, if the concentration of anti-angiogenic treatment was increased enough. The increase in the emigration strategy also abated since the effect of the treatment disappeared in the absence of angiogenesis.

The anti-angiogenic treatment did not necessarily lead to non-viability since the baseline resource inflow $\hat{R}$ kept the population viable. However, if the population was originally non-viable (insufficient $\hat{R}$), increasing the anti-angiogenic treatment enough would lead the population back to non-viability.

Cytotoxic treatment increased the death rate. Consequently the populations were smaller and cells were more likely related. In such situation both angiogenesis and emigration were favored based on kin selection. However, as noted in the beginning of Section 3.3.2 the increase in one strategy component decreased the other. In the joint evolution, the indirect effects could cause such phenomenon when increasing the cytotoxic treatment. However, the direct effects of cytotoxic treatment dominated, and both strategy components increased. The average emigration rate initially increased along with emigration and angiogenesis strategies, but started to decrease and approach the emigration strategy. This happened since the increase in treatment decreased the average population size and eventually there were no cells left to contribute to angiogenesis. Thus, regardless of the angiogenesis and emigration strategies, the population became non-viable when the cytotoxic treatment was high enough.

Combination of anti-angiogenic and cytotoxic treatments

Both monotherapies have their downsides, as anti-angiogenic treatment does not lead to non-viability and cytotoxic treatment would be preferred at minimal effective doses due to side effects. Therefore, we investigated whether the combination

treatment would overcome these downsides.

Similarly to the cytotoxic monotherapy, the population eventually became non-viable when cytotoxic treatment was increased despite the increase in the angiogenesis and emigration strategies (Fig. 14). Compared with the cytotoxic monotherapy (Fig. 14a) the combination therapy (Fig. 14b) lowered the need of cytotoxic treatment as the non-viability was reached with smaller ψ_c. The concentration of anti-angiogenic treatment affected how much the need for cytotoxic treatment decreased. However, increasing the anti-angiogenic treatment started to lose its benefit and almost equal result could already be achieved with lower level of anti-angiogenic treatment. A lower treatment level would also be preferred considering the additional costs of combination therapy. See also Section 3.3.3 for the emergence of treatment resistance.
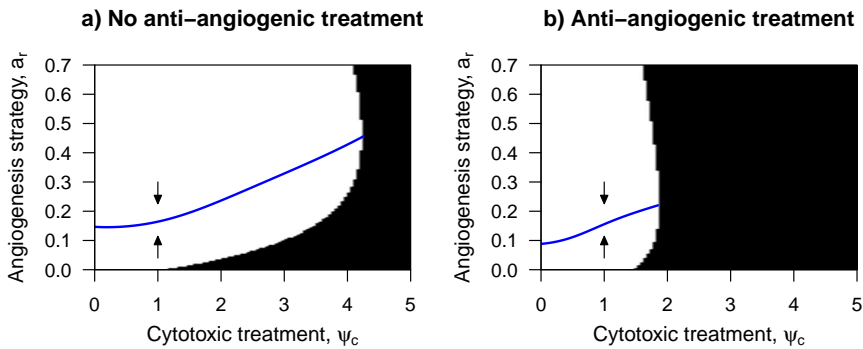
Figure 14. Angiogenesis strategy (blue line) at the joint singular strategy of angiogenesis and emigration with respect to cytotoxic treatment a) without anti-angiogenic treatment and b) with anti-angiogenic treatment. Black area denotes non-viability. (Adopted with permission from Publication II: Fig. 7a and b.)

3.3.3 Joint evolution with treatment resistance

We considered the joint evolution of treatment resistance, angiogenesis and emigration strategies. Since the resistance was modelled against the anti-angiogenic treatment, we focused on how that treatment affected the joint singular strategy and especially the treatment resistance.

Bistability scenario

For the selected parameter values, the number of singular strategies depended on the concentration of anti-angiogenic treatment (Fig. 15a). For small concentrations, a single attracting singular strategy existed with no treatment resistance. An additional

singular strategy with positive resistance was detected for higher treatment levels. Between the two attracting singular strategies, there was a saddle point. The stable manifold of this saddle point determined the areas in the strategy space from which the strategies evolved to each attracting singular strategy. The maximum treatment effect without a high risk of resistance would be before the positive resistance singular strategy appears (around 3.8 in Fig. 15a).

We further investigated a situation, where the resident population was not treatment resistant despite the anti-angiogenic treatment ($\psi_a = 7$). The angiogenesis and emigration strategies were at their joint singular strategy corresponding to the selected treatment. For such resident, the resistance strategy component had a negative fitness gradient (black dot and arrow in Fig.15b). Since the resistance strategy had to be non-negative, it was likely to remain in zero. However, some variants with multiple radical variations could invade (area of positive fitness in Fig. 15b).
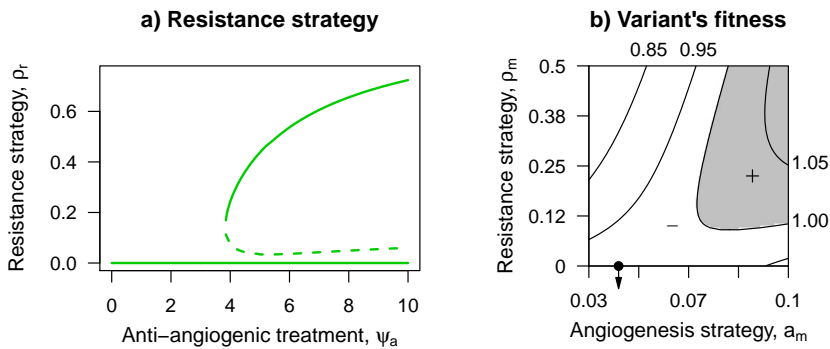
Figure 15. a) Resistance strategy at the joint singular strategy of all three strategies. The solid lines are attracting singular strategies, the dashed is repelling singular strategy. b) Slice of the 3D fitness matrix calculated with respect to resident's strategy (black dot). Here $e_m = e_r$. The arrow points the direction of fitness gradient from the resident's strategy. The black lines are contour lines for different fitness values. (Panel a adopted with permission from Publication II: Fig. 8a.)

The effect of cytotoxic treatment

As noted in the previous section, the anti-angiogenic treatment did not necessarily lead to treatment resistance, even if the concentration was increased. If the combination of anti-angiogenic and cytotoxic treatment was used, the bistability of singular strategies was present only for a narrow range of treatment regimens. The singular strategy with zero resistance was repelling for a wide range of treatment combinations leading to the emergence of treatment resistance. Compared to the anti-angiogenic monotherapy, a lower average population was reached with the combination, despite the higher risk of treatment resistance. However, as in the previous

sections, the combination treatment might come with additional burden for the patient.

In addition to treatment parameters, the bistability with anti-angiogenic monotherapy shifted or disappeared when other parameters were changed. For example, when decreasing the resistance trade-off on birth rate (β), resistance strategy became more profitable for cancer cells and, therefore, a positive resistance was attained even with smaller treatment concentration.

4 Cancer survival prediction based on clinical data

In Publication III, cancer survival was predicted with two methods: LASSO selection and a greedy budget-constrained Cox regression (Greedy Cox). In Publication IV, a new method OSCAR (Optimal Subset CArdinality Regression) was presented for penalized (Cox) regression. In both Publications the aim was to provide new tools for better prediction while simultaneously considering the model sparsity. The model sparsity was also desired, since in real life applications the cost of measuring the parameter values may considerably increase along with the number of predictors. In both Publications III and IV, the cost aspect was considered with real life data from advanced prostate cancer.

4.1 Literature review

Prognostic modelling is used to aid the prediction of cancer survival and assessing who may benefit from a certain treatment regimen. Fitting the model into a data set results in model coefficient values that can then be used to form predictions for new patient data. An additional data can be used to further train the model to better fit a target population. For survival prediction, Cox regression [9] has been widely used as the base of modelling. In the Cox's proportional hazards model, the hazard is

$$h(t, \boldsymbol{x}) = h_0(t)e^{\beta^\top \boldsymbol{x}}, \tag{27}$$

where $h_0(t)$ is a shared baseline hazard, $\boldsymbol{x}$ is a feature vector and β is the coefficient vector.

Furthermore, to prevent over-fitting and enable model sparsity, penalized Cox regression [93; 94] has been applied. For example, in the DREAM 9.5 Challenge for survival prediction of metastatic castration-resistant prostate cancer (mCRPC), the top model was based on an ensemble-based penalized Cox regression model (ePCR, [95]). In addition to penalized methods, different approaches, such as other statistical, Bayesian, neural network or random forest methods have also been utilized to ensure model sparsity (see e.g. [96; 97; 98; 99; 100; 101; 102]).

For penalized Cox regression, most commonly used penalization terms are L_1-norm (LASSO), L_2-norm (ridge regression) or their sum (elastic net) [103]. Both L_1 and L_2 push coefficients (β_i) towards zero, however, L_1 selects only some nonzero

coefficients, while L_2 tends to set none to exactly zero. L_1 has difficulties with highly correlated parameters, selecting only one of them. L_2 tends to give correlated parameters an equal coefficient value. Elastic net combines the two so that the penalization to be minimized is

$$\lambda \left(\alpha \sum |\beta_i| + (1 - \alpha) \sum \beta^2 \right), \tag{28}$$

where the first term is the effect of L_1 and the latter is the effect of L_2. Here α determines the trade-off between L_1 and L_2, and λ can be altered to tune the amount of penalization. For example, Halabi et al. [99] and Goeman [104] utilized LASSO-penalty, while Simon et al. [94] and Guinney et al. [95] considered elastic net with varying α. Also Meier et al. [100] tested between the three penalties. In Publication III, both L_1 (LASSO selection) and L_2 (Greedy Cox) were included.

However, another option for L_1 and L_2 is to restrict the number of predictors with L_0-pseudonorm, which calculates the number of nonzero coefficients. Unlike L_1 and L_2, L_0 is not considered a proper norm since it is non-homogeneous [105]. In addition, it is discontinuous and noncovex, which leads to challenging, NP-hard (nondeterministic polynomial hard) optimization problem [106; 107; 108; 109]. This has led to under-presentation of L_0 in the penalized regression. A few L_0-approaches are implemented into R-packages, that include generalized linear models with linear and logistic regression [110; 111]. A model, augmented penalized minimization-L_0 (APM-L_0) [112] augments L_0 for Cox's proportional hazards model. However, the L_0 is approached indirectly through minimizing the L_0-pseudonorm of surrogate coefficients, which are compared to the actual coefficients used in the hazards model. In Publication IV, the L_0-pseudonorm was used directly in the optimization of model coefficients. An exact, continuous representation of L_0 [107] was included as a cardinality constraint that limits the nonzero coefficients.

In addition to differences in the penalty functions, the actual model fitting has been done with different methods. One popular approach is to use coordinate descent in the optimizing the selection of coefficient values. Coordinate descent has been utilized by, for example, Simon et al. [94] and Li et al. [112]. Goeman [104] combined gradient ascent and the Newton-Raphson algorithm. Our approach with L_0-pseudonorm resulted in a continuous exact representation of the penalization term, which is also a DC function (difference of two convex functions). The DC structure may be exploited in the optimization and thus we used DBDC (the double bundle method) for DC optimization [113; 114]. DBDC suits the problem also since the L_0 representation is still nonconvex. Another optimization algorithm LMBM (the limited memory bundle method) [115; 116] was included as an option for larger problems, however, LMBM does not utilize DC structure.

In Publication III and IV, the presented methods were applied on prostate cancer data.

As the prostate cancer is one of the most common cancers among men [1; 117], it is a relevant subject for prognostic prediction. Furthermore, the need for cost-efficiency of prediction was considered in both Publications, since the application of models requires money. Some parameter values are also often measured as groups or kits like basic blood count, which includes hemoglobin, white blood cells and red blood cells, among others. In both Publications III and IV, the kit structure was included.

4.2 Materials and methods

Concordance index (C-index) [118] was used as the measure of model performance in both Publications III and IV. In Publication III, also integrated AUC [119] was calculated for supplementary analyses to enable comparison to previous research. Cross-validation was used to further evaluate the model selection. For Publication IV also bootstrap analysis was performed to interpret which features were the most robust.

4.2.1 Data

We tested our survival prediction methods in four prostate cancer cohorts. Three data cohorts, MAINSAIL, VENICE and ASCENT [120; 121; 122], were from randomized clinical trials and one data cohort was from real-world hospital registry data. The clinical trial data were constructed in the DREAM competition (the Prostate Cancer Challenge, PCC-DREAM), hosted by Project Data Sphere [123]. In Publication IV the trial cohorts were divided into validation (N=132, N=150 and N=119 for MAINSAIL, VENICE and ASCENT respectively) and training sets (N=394, N=448 and N=357 respectively). Missing values were imputed separately for each cohort using the median values calculated from the training sets.

The real-world hospital registry data were collected from patients with castration resistant prostate cancer treated at the Turku University Hospital (TYKS). The data was processed as in [124]. For Publication III, only variables with less than 40% of missing values were selected. The missing values were imputed using medians as the median imputation has previously given satisfactory results [124]. The k-nearest neighbor imputation was also tested, however it did not improve model performance.

For Publication IV, the patients with diagnosis date before 2010 were discarded due to high percentage of missing values. Unlike in Publication III, only laboratory measurement data and the age group information were included. Furthermore, the features with more than 50% of missing values were discarded. Similarly to the trials data, TYKS cohort was divided into validation set (N=195) and training set (N=590). The remaining missing values were imputed using medians calculated from the training data.

In both Publications III and IV the features were also considered as groups or kits in which the features are measured together. Prices for the examinations were provided by the Helsinki University Hospital. The prices were scaled in relation to PSA, which was given a reference value of 100.

For both Publication III and IV the initially same four data cohorts were tested in survival prediction, however, the data were processed slightly differently and different features were included. In addition, for Publication IV, the TYKS data was updated to include new patient data that had been collected after the analyses performed for Publication III.

4.2.2   LASSO selection and Greedy Cox methods

In Publication III the approaches were based on Cox regression [93] with either L_1 (LASSO) or L_2 (ridge regression) penalization. Penalization was varied to determine the sparsity and select different sets of variables. In the Cox's proportional hazards model (27), the coefficients β were selected by maximizing the penalized partial log likelihood [103].

We denoted the set of available variables with F, and formed subgroups G_i that included the variables measured in kit i. Variables measured on their own were considered as groups containing one variable. A variable was allowed to belong to multiple subgroups (e.g., hemoglobin individually or as a part of blood count). A group was also allowed to be included partially, with only some of the group variables in the model. Selected model variables were denoted by $S = \bigcup_{i \in I} s_i$, where I is the group indices included in the model and s_i are the variables selected from the group G_i. The price of the group G_i was denoted by c_i and the cost for a model was calculated by $C = \sum_{i \in I} c_i$. The cost was not reduced by exclusion of some variables in a selected group since the group was measured as a whole regardless of how many of its variables were included in the model.

Since the price of measuring the selected variables is not included in the LASSO method, the price was computed afterwards using a heuristic that added variable groups sequentially. Groups were added until all selected variables in S were included. At each step, the group with the smallest cost per new variable was selected.

However, we also proposed an alternative, a greedy budget-constrained Cox regression (Greedy Cox) algorithm. The algorithm sequentially selects the variable group that, with already selected variables, gives the best cross-validated (threefold) model performance estimate. Since an added group may have also unfavorable variables, an inner selection is performed on the variables of the considered group. The mechanism of inner selection of individual variables is similar to the group selection. The selection of new groups is stopped if the budget does not fit any of the remaining groups or the addition does not improve prediction performance. Unlike LASSO with L_1-penalization, Greedy Cox utilizes L_2-penalization.

At the initialization, S is initialized as an empty set and the remaining budget is set to the total budget. The group selection step, followed by inner selection, require the matrix of clinical variable measurements of the patients and the survival data, i.e. time and type of event (death or right-censoring). In addition, the input should include the remaining budget, variable groups G_i and their prices C as well as already selected variables S and the selected group indices I. The group and inner selections return the index i of the selected group and the variables s_i selected from that group. The remaining budget, S and I are then updated. The group and inner selections are called repeatedly until the budget does not fit any new groups that improve the performance.

4.2.3   OSCAR method

The OSCAR method presented in Publication IV implements the penalized Cox regression [93]. However, unlike LASSO selection and Greedy Cox in Publication III, the OSCAR method utilizes L_0-pseudonorm in the penalization. In addition to Cox regression and survival prediction, the OSCAR method includes also logistic and linear regression for prediction of binomial and scalar responses. Similarly to the methods in Publication III, the OSCAR method can consider the features either separately or grouped into kits. The OSCAR method was implemented utilizing Fortran, C and R and it is available as an R package OSCAR in the Central R Archive Network (CRAN) at: `https://CRAN.R-project.org/package=oscar`.

In Cox's proportional hazards model [9] the hazard for the patient i at time t is $h_i(t) = h_0(t)e^{x_i^\top \beta}$, where $h_0(t)$ is a shared baseline hazard, x_i is the vector of observed features and β is the vector of predictor coefficients. In the OSCAR method, the vector β is estimated by maximizing the scaled log partial likelihood, which leads to an equivalent solution as the Breslow approximation of partial likelihood [125; 94]. The scaled log partial likelihood is

$$l(\boldsymbol{\beta}) = \frac{2}{n} \sum_{i=1}^{m} \left\{ \sum_{j \in D_i} x_j^\top \boldsymbol{\beta} - d_i \ln \left(\sum_{j \in R_i} e^{x_j^\top \boldsymbol{\beta}} \right) \right\}, \tag{29}$$

where n is the number of observations and m is the number of unique event times. Furthermore, R_i is the set of patient indices at risk and D_i is the set of indices with the label equal to one at time t_i. As the label equal to one indicates an event (death) and zero indicates right-censoring, $d_i = |D_i|$ is the number of events at time t_i. Maximizing the concave function l is the same as minimizing the convex function $-l$ [126].

The minimization problem is modified further to include the regularization and enable model sparsity. The L_0-pseudonorm is included as a cardinality constraint

that restricts the number of nonzero predictors in $\boldsymbol{\beta}$. Unlike in LASSO, the values of nonzero coefficients in $\boldsymbol{\beta}$ are not penalized and are allowed to vary freely.

The L_0-pseudonorm $\|\boldsymbol{\beta}\|_0$ calculates the number of nonzero components, and it gives the cardinality constraint $\|\boldsymbol{\beta}\|_0 \leq K$. However, since the constraint is discontinuous, we used an approach [107] with the largest-k norm to form an exact continuous representation. The constraint $\|\boldsymbol{\beta}\|_0 \leq K$ is replaced by the equivalent constraint $\|\boldsymbol{\beta}\|_1 - \|\|\boldsymbol{\beta}\|\|_{[K]} = 0$ [107; 106]. Here $\|\|\boldsymbol{\beta}\|\|_{[K]}$ is the largest-k norm, which is the sum of the k largest absolute value elements in $\boldsymbol{\beta}$. Thus, the optimization problem is rewritten as

$$\begin{cases} \min_{\boldsymbol{\beta} \in \mathbb{R}^p} & -l(\boldsymbol{\beta}) \\ \text{s.t.} & \|\boldsymbol{\beta}\|_1 - \|\|\boldsymbol{\beta}\|\|_{[K]} = 0. \end{cases} \tag{30}$$

The constraint is continuous but also noncovex due to its combinatorial structure. The constrained optimization problem in (30) is rewritten as an unconstrained problem [127; 128]

$$\min_{\boldsymbol{\beta} \in \mathbb{R}^p} \quad f(\boldsymbol{\beta}) = -l(\boldsymbol{\beta}) + \rho \left(\|\boldsymbol{\beta}\|_1 - \|\|\boldsymbol{\beta}\|\|_{[K]} \right) \tag{31}$$

where ρ is a positive penalization parameter. By suitably large ρ the original constraint in (30) is forced to hold.

The objective in (31) is nonconvex and nonsmooth, but it is also a DC function (Difference of two Convex functions) and can be represented as $f = f^1 - f^2$, where

$$f^1(\boldsymbol{\beta}) = -l(\boldsymbol{\beta}) + \rho\|\boldsymbol{\beta}\|_1 \quad \text{and} \quad f^2(\boldsymbol{\beta}) = \rho\|\|\boldsymbol{\beta}\|\|_{[K]}.$$

Here the functions f^1 and f^2 are convex.

The optimization problem (31) is solved with the new OSCAR algorithm presented in Publication IV. Since the objective is DC, the algorithm utilizes the double bundle method (DBDC) for DC optimization [114; 113]. The starting points for DBDC are generated with and incremental approach. Solving the problem starts with allowing only a single predictor (or kit) to be selected into the model. Then the number of predictors (or kits) is increased until the maximal number of predictors (or kits) is reached. The solution for the cardinality-constrained problem with $k - 1$ predictors is used to derive promising starting points for the problem with k predictors. Since such selection may fall in local optimum, we use several starting points and, from the resulting solutions, the best is selected.

Similarly to Greedy Cox in Publication III, the OSCAR algorithm requires the input matrix including the observed patient features and the survival data (time and event/right-censoring) in case of the survival prediction. If logistic or linear regression is used, a vector of responses should be given instead. Additionally, the maximum number of predictors K needs to be defined. If not given by the user, it is

calculated from the feature matrix in the R interface. A kit matrix may also be given to fit the features as groups.

In the algorithm, the solution is initialized by solving the unconstrained problem $-l$ with DBDC. Starting from $k = 1$ the starting points are constructed by varying the previous solution β_{k-1}^* (or the initialized solution in case of $k = 1$). Then for all starting points the problem (31) is solved with DBDC method. The penalization parameter is increased if the cardinality-constraint is not satisfied. The best solution is selected from the solutions obtained from different starting points. The steps are repeated up until the problem with cardinality $k = K$ is solved. The algorithm returns the solutions (i.e., the vectors β) for each cardinality-constrained problem with $k = 1, \ldots, K$ predictors.

In addition to DBDC, the method can use other solvers that are capable to handle nonsmoothness and nonconvexity. In our R package, we included also the limited memory bundle method (LMBM) [115; 116], which can be used in optimization instead of DBDC. LMBM is for general nonconvex and nonsmooth minimization problems and it can handle large-scale problems. However, unlike DBDC, LMBM does not benefit from the DC structure.

4.3 Results

4.3.1 LASSO selection and Greedy Cox

The methods (LASSO selection and Greedy Cox) were tested in the four data cohorts TYKS, VENICE, MAINSAIL and ASCENT (TYKS was named RWC, i.e. real-world cohort). Different training and testing data combinations were tested. If the training and testing data were from the same cohort, subsets of the cohort were assigned to either training or testing set. C-index was calculated either for a single fitting or cross-validation.

The budged was varied, and for low budgets Greedy Cox gave better results. In cross-validation, the highest model performance was usually reached with LASSO selection. However, if the budget was further increased, the performance of LASSO selection deteriorated while the results of Greedy Cox stayed on the same level. This may be because in LASSO selection the penalization is reduced to obtain sets with higher budget while Greedy Cox has fixed penalization. However, with Greedy Cox, a small increase in a low budget might result in lower model performance since with the increased budget, an expensive variable group was selected first with no money left for other non-free variables. If a lower budget was given, the first variable group had to be less expensive and another low-cost, but non-free, group could be selected as well. Peak model performance was achieved with a budget around 200-400 with usually 10-15 variables.

In TYKS cohort with an unlimited budget, Greedy Cox selected prostate-specific

antigen (PSA) as the first predictor followed by the group of hemoglobin (HB), white blood cells (WBC), ratio of lymphocytes and leukocytes (LYMperLEU) and ratio of neutrophils and leukocytes (NEUperLEU). In the third step alkaline phosphatase (ALP) was selected in addition to the previous variables. Also LASSO selection started with PSA, HB, ALP and the age group (AGEGRP) (four steps in total). With more steps, the order of selected variables started to differ between the two methods. In Figure 16 the results are presented in relation to the costs and C-indices (until the budget is 300). In the trial cohorts the selected variables varied, however, lactate
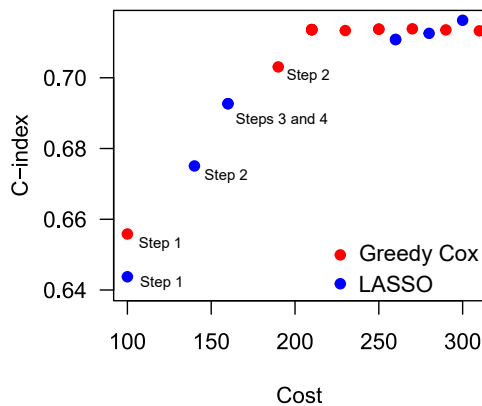
Figure 16. The C-index in TYKS cohort with respect to cost when the model was fitted with Greedy Cox (red) or LASSO selection (red). The budget was unlimited for Greedy Cox and the cost was calculated afterwards.

dehydrogenase (LDH) was selected in all trial cohorts with both Greedy Cox and LASSO selection. However, LDH was not available in TYKS cohort. Most likely variables to be selected in trial cohorts were LDH, HB, ALP, PSA and whether the patient had suffered congestive heart failure (CHF). From these, PSA, HB and ALP were also prominent predictors in TYKS cohort.

In addition, models for selected budgets were further investigated with the ePCR package [124] after the variables were first selected by LASSO selection or Greedy Cox. The further analysis with ePCR was conducted to optimize the amount of penalization (e.g. λ in Eq. (28)). Since the ePCR package can construct ensemble models combining results of multiple models, some ensembles were also investigated for models fitted in different data cohorts. For example, when tested in TYKS cohort, the best model was fitted in VENICE cohort with variables selected by LASSO selection (Fig. 17). See Supplementary of Publication III for more details.

Figure 17. Integrated AUC for models tested in TYKS cohort. Models were either fitted to VENICE cohort or VENICE, MAINSAIL and VENICE + MAINSAIL for ensemble models. Two different budgets are shown (190 and 380). Variables were first selected by 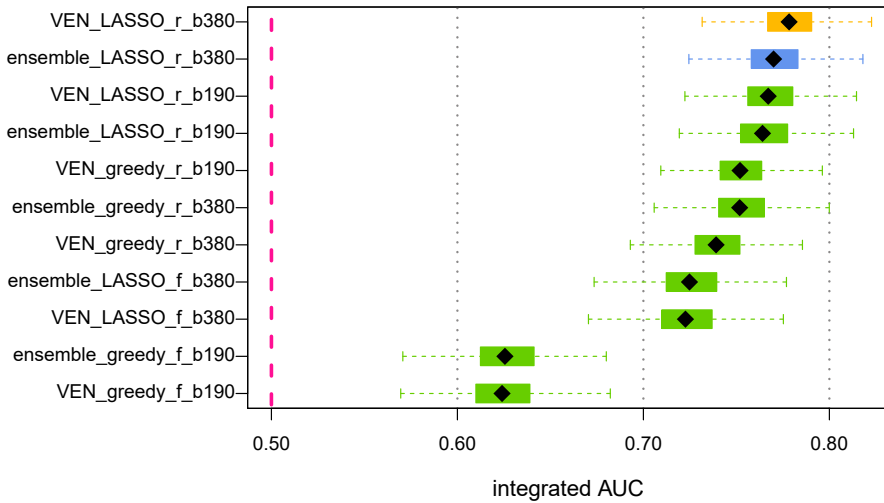LASSO selection or Greedy Cox in the VENICE cohort. The letter 'f' indicates that the full set of variables was allowed, and the letter 'r' indicates that the set was reduced to those with less than 40% of missing values in TYKS cohort. The colors indicate Bayes factors (BF) calculated to compare the models to the top model (yellow): $BF < 20$ (blue), $BF \geq 20$ (green). (Adopted with permission from Publication III: Suppl. Fig. 3.)

4.3.2 OSCAR

We tested the OSCAR method in the four data cohorts and analyzed the results obtained from fitting into the training data (C-index), cross-validation and bootstrap analysis. In addition, we investigated, which models were cost-efficient (i.e., maximum accuracy, minimal cost), thus making the underlying problem a multi-objective optimization problem. We obtained an approximation of the Pareto-front from cross-validation C-index and costs for corresponding cardinalities in the training data fit. We further tested the models of the approximated Pareto-front in the validation sets separated from the data before model fitting. We also compared the OSCAR method to LASSO and APM-L_0 [112]. See Figure 18 for the schematic illustration of the method and the post-fitting analyses.

In the TYKS cohort the PSA was the most robust predictor and in the bootstrap analysis it was selected most often if only one predictor was allowed. HB, ALP and age group were also promising predictors and the C-index improved when compared to the PSA alone (0.654 vs 0.726). The cost also remained low with these predictors (100 with only PSA vs. 160 with the four predictors). The model accuracy did not dramatically improve with more predictors (maximum 0.735 in training data). In
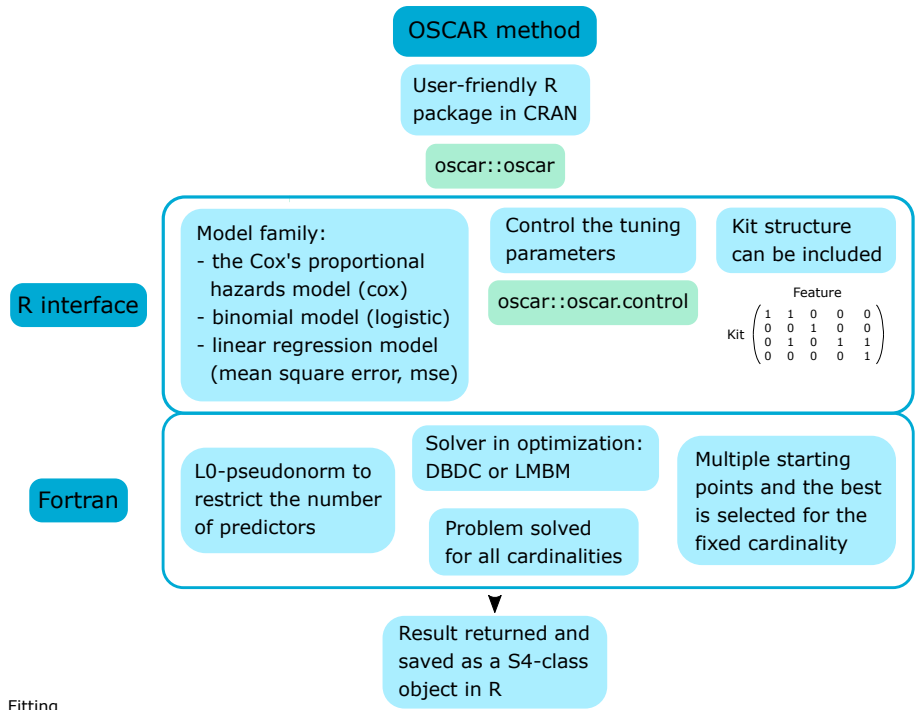
Figure 18. Schematic illustration of the OSCAR method and post-fitting analyses. The bottom panel results are from simulated real-world registry data included in the R package. (Figure adopted with permission from Publication IV: Fig. 1.)

comparison to LASSO and APM-L_0, all three methods selected similar predictors, e.g. PSA, HB and ALP. However, in the cross-validation, OSCAR resulted in higher mean C-index than LASSO and APM-L_0. This might be due to OSCAR method not penalizing the values of selected model coefficients, unlike LASSO which pushes coefficients towards zero.

The cross-validation results were also investigated against the costs and, within a selected cost, the OSCAR performance was the highest when compared to the other two methods. The approximated Pareto-fronts (min cost, max accuracy) are presented in Fig. 19. The models of the approximated Pareto-fronts were tested in validation data and similar accuracy was reached when compared to the training data (C-index around 0.70-0.73). If the kit structure was included, PSA was selected first, followed by B-PVKT kit (basic blood count and trombocytes) consisting here of HB, platelets (PLT), WBC, RBC and hematocrit (HEMAT). In this application, the model performance was on a similar level than without the kit structures. However, including a kit with highly prognostic feature (like HB in the B-PVKT) might have less prognostic features that are included as well.
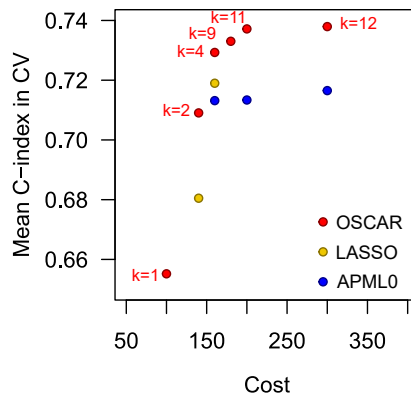
Figure 19. The cross-validation mean C-indices against the costs for the approximated Pareto-front models obtained with OSCAR (red), LASSO (yellow) and APM-L_0 (red). The cardinalities are marked for OSCAR. For LASSO the numbers of predictors are 2 and 4 starting from left, and corresponding numbers for APM-L_0 are 4,6 and 14.

In trial cohorts (VENICE, MAINSAIL, ASCENT) the most robust predictors varied. Unlike in TYKS, PSA was not as robust and, based on bootstrap analysis, it was selected often only in ASCENT. If only one predictor was allowed, ALP was selected most often in ASCENT and VENICE cohorts. In MAINSAIL, LDH was the most robust predictor. HB was relevant predictor in VENICE and MAINSAIL. In the VENICE cohort, potential additional predictors were aspartate aminotransferase (AST), creatinine (CREAT), sodium (NA) and albumin (ALB). In the MAINSAIL cohort magnesium (MG), body mass index (BMI), ALB, AST and weight were po-

tential predictor candidates. In the ASCENT cohort neutrophils (NEU), calcium (CA), LDH and HB were selected often in the bootstrap analysis.

When compared to LASSO and APML-L_0, all three suggested similar predictors. However, like with TYKS cohort, in the cross-validation analysis, the OSCAR method resulted in higher mean C-index than LASSO and APM-L_0. Similarly to TYKS, the Pareto-front was approximated from cross-validation mean C-index and costs and OSCAR resulted in higher accuracies when compared to LASSO and APM-L_0 within the same cost. The models of the approximated Pareto-fronts were tested in the validation data. Considering the objective of maximizing C-index and minimizing the cost, OSCAR performed well in the validation data.

5 Discussion

Previous chapters summarize the approaches that were investigated to obtain predictions of cancer behavior and treatment outcomes. Publications I and II have more theoretical mechanistic approaches to achieve qualitative predictions of cancer behavior. Publications III and IV lean towards machine learning with training data and patient outcomes.

The ODE model in Publication I (Chapter 2) incorporates the key aspects of cancer and immune system communication: activation and infiltration of T-cells, elimination of cancer cells and cancer cells making T-cells inefficient. In addition, the immunotherapy was incorporated with targeted and chemotherapy. The model could be easily altered for different patients to form an individualized model to make patient-specific predictions and treatment decisions. For example, the cancer cells' sensitivity to either the T-cell attack (antigen missing) or different treatments could be tailored. Also, it is possible to further develop the model and include other immunotherapy mechanisms, such as the lack and treatment of the initial T-cell activation (CTLA4 vs. anti-CTLA4).

In Publication I, different immunotherapy schedules were compared with each other (pre-set treatment periods vs. threshold-based treatment initiation), and it was noted that both have their advantages and disadvantages. However, the threshold-based initiation led to a positive treatment outcome (low cancer burden) more easily, as the treatment schedule responded to the need rather than sticking to a pre-set schedule that might not have been suitable.

On the other hand, the pre-set periods may also be adapted to an extent, by starting with a tighter schedule and lengthening the drug holidays (gaps between treatments) later, when the initial treatment response is already achieved. In general, the treatment combinations, with either immuno- and targeted therapy or immuno- and chemotherapy led to a better treatment effect than monotherapies, however, despite the additional possibility of fewer treatment initiations, the burden of two therapies has to be considered. With careful treatment selection and based on the underlying biological patient characteristics, a stable, possibly undetectable, disease was attainable [42; 43; 44; 45] or cancer remained chronic with repeated treatment periods [129].

The metapopulation model in Publication II (Chapter 3) adapted some aspects present in the Publication I (e.g., the resources), however, instead of the immune response, the process of angiogenesis was incorporated. Also, instead of investigating the treatment effect on non-variating cancer cell subpopulations (Publication I), the metapopulation model was utilized to investigate the change in the populations, i.e., how the different treatment regimens affected the qualities of the population. We investigated the treatments' effect using tools of adaptive dynamics [63; 64; 65] and analyzed how the cells' angiogenesis contribution, emigration eagerness and resistance against anti-angiogenic treatment would evolve under the treatments. A positive angiogenesis contribution was shown to be beneficial for cancer cells if the benefits outweigh the costs [66; 67]. Similarly to real-life observations, the anti-angiogenic monotherapy did not usually extinguish cancer completely and combination treatments were required [17; 80; 81]. The main focus was on the anti-angiogenic therapy, however, we modelled and analyzed also cytotoxic treatment. It was observed that the combination with anti-angiogenic treatment reduced the need for cytotoxic treatment when the goals was to reach population non-viability. The treatments and their dosages have to be carefully selected to avoid high risk of treatment resistance while maintaining sufficient treatment effect.

Both immune response and angiogenesis play an important part in the cancer development, the previous being the body's own attempt to eradicate the anomaly, and the latter being the key hallmark to achieve a higher level of cancer growth. Thus it would be interesting to connect these key phenomena present separately in Publications I and II into a combined model. Since both of these models also incorporate resources, it would be interesting to include the cancer cells' ability to adapt to low level of resources or hypoxia [130; 131]. The emergence of new (resistant) variants often causes the relapse and treatment failure [132], and thus it would be interesting to investigate it also in the ODE model in Publication I. Multiple dynamically adapting populations could be included, also to present normal or endothelial cells. Also the treatment mechanisms could be expanded to include a combination of multiple immune response mechanisms and corresponding therapies (e.g., anti-PD1 and anti-CTLA4), or a combination of multiple angiogenesis mechanisms and therapies, such as VEGF family and fibroblast growth factors (FGFs) [33]. In the case the angiogenesis and immune response mechanism were combined, the combination therapy of anti-angiogenic treatment with immunotherapy could be considered [82; 83].

In Publications III and IV (Chapter 4) the cancer survival was predicted with methods based on penalized Cox regression [9; 93]. It was noted that the economic costs could be reduced without a great loss in prediction accuracy. In Publication III, Greedy Cox algorithm performed better than the LASSO selection, when the budget was low, however, overall the LASSO selection gave the highest accuracy. Even though not completely comparable due to slight differences in the training data, OS-

CAR method in Publication IV produced similar or slightly higher level of accuracy as the methods in Publication III. For Greedy Cox and OSCAR, the grouped structure (kit structure) of features was included to accommodate the real-world practice of measuring the features together (e.g. complete blood cell count).

The methods in Publication III used traditional L_1 and L_2 penalizations, however, for Publication IV we implemented L_0-pseudonorm, which is discontinuous and noncovex, making the optimization problem NP-hard [108]. The penalization term was rewritten to an exact continuous presentation which was also in the form of a DC composition. This enabled the use of DBDC algorithm [113; 114] in the optimization. L_0-pseudonorm also allowed the nonzero model coefficients to vary freely away from zero (unlike, e.g., in LASSO).

We investigated the model performance in four data cohorts, one from hospital registry data (TYKS) and three from randomized clinical trials (VENICE, MAIN-SAIL, ASCENT). For TYKS data, all tested methods resulted in similar main predictors: PSA, HB, ALP and AGEGRP. If the number of predictors (or budget) was increased, the selected predictors started to vary. For trial cohorts, methods in Publication III selected predictors such as LDH, HB, ALP, CHF and PSA. These were distinguished also with OSCAR method: ALP, AST, CREAT, NA, HB and ALB for VENICE; HB, ALB and LDH for MAINSAIL; PSA, ALP, LDH and HB for ASCENT. Some of the detected differences between cohorts and methods may be due that in Publication III, there were more features from which to select. In addition, some important predictors selected in trial cohorts were not available in TYKS cohort. However, the selected parameters are reasonable and validate the method functionality, when compared to previous research (e.g. [95]) and clinical practice. For example, PSA reflects the disease severity and has been assessed as an important predictor of disease state [133]. Furthermore, ALP is associated with metastases in prostate cancer [134]. LDH is released by damaged tissues and has been linked to cancer [135].

Since the cost was calculated after the model fitting for OSCAR and LASSO selection, in future work it would be an interesting challenge to incorporate the cost as a part of the objective function. This would require the inclusion of discrete coefficients in the optimization. The selection of starting points in OSCAR method affects the outcome and also the running time, thus further development on the starting point selection would be interesting and potentially beneficial for the overall applicability.

6 Conclusions

We modelled cancer dynamics with an ODE model incorporating the mechanism of immune response and immunotherapy. We predicted the treatment outcome of different treatment regimens, either as monotherapies or in combinations. Different scheduling techniques were also compared to see whether the pre-set treatment periods usually used in practice would be outperformed by a threshold-based treatment initiation. Generally, a more adaptive schedule, either with a threshold-initiation or modifying the pre-set treatment schedule, resulted in smaller cancer burden along with less time in treatment. We also considered cancer in a continuous-time metapopulation model with migration through a dispersal pool. A mechanism of angiogenesis and anti-angiogenic treatment was included and, using the tools provided by adaptive dynamics, we investigated how the cancer cells affect the angiogenesis depending on the treatment. We also analyzed the evolution on emigration and treatment resistance against anti-angiogenic treatment.

Three variable selection methods were implemented and tested, one being a cost-specified greedy algorithm (Publication III), one based on LASSO regularization (Publication III) and one based on L_0-pseudonorm regularization with DBDC optimization (Publication IV). All three methods (LASSO selection, Greedy Cox and OSCAR) were designed to achieve prognostic models with varying levels of sparsity to monitor, not only the prediction accuracy, but also the cost-efficiency. For Greedy Cox, the budget was incorporated into the algorithm, whereas the other two methods consider the cost afterwards. Group-wise feature selection was included in Greedy Cox and OSCAR since group-wise measurement of features is general practice in clinic. Greedy Cox and LASSO selection restrict the model parameters with well-known L_2 and L_1 penalizations. The L_0 penalization in OSCAR method has been under-represented in regularized regression due to its discontinuous and nonconvex nature. OSCAR method utilizes an exact DC-composition of the penalty term. OSCAR method was also made available as a user-friendly R package in CRAN. We tested and validated the methods in prostate cancer patient data (real-world and trial cohorts), which is clinically significant due to high occurrence among men.

We have presented highly applicable models and methods with varying approaches and key aspects (i.e. angiogenesis and immune response) to gain insights into the

cancer development and response as well as the patient survival prediction. We have incorporated multiple treatment options in the theoretical models and analyzed the qualitative outcomes. We utilized a real-world and trial data cohorts from advanced prostate cancer to predict the overall survival with three penalized regression methods. Hopefully these novel models and methods lead to more patient-specific treatment choices and bring new tools into the quest of defeating cancer.

List of References

[1] Hyuna Sung, Jacques Ferlay, Rebecca L. Siegel, Mathieu Laversanne, Isabelle Soerjomataram, Ahmedin Jemal, and Freddie Bray. Global Cancer Statistics 2020: GLOBOCAN Estimates of Incidence and Mortality Worldwide for 36 Cancers in 185 Countries. *CA: A Cancer Journal for Clinicians*, 71(3):209–249, 2021. ISSN 0007-9235. doi: 10.3322/caac.21660.

[2] Ivana Bozic, Johannes G. Reiter, Benjamin Allen, Tibor Antal, Krishnendu Chatterjee, Preya Shah, Yo Sup Moon, Amin Yaqubie, Nicole Kelly, Dung T. Le, Evan J. Lipson, Paul B. Chapman, Luis A. Diaz, Bert Vogelstein, and Martin A. Nowak. Evolutionary dynamics of cancer in response to targeted combination therapy. *eLife*, 2013(2):1–16, 2013. ISSN 2050084X. doi: 10.7554/eLife.00747.

[3] Ivana Bozic and Martin A. Nowak. Timing and heterogeneity of mutations associated with drug resistance in metastatic cancers. *Proceedings of the National Academy of Sciences*, 111(45): 15964–15968, 2014. ISSN 0027-8424. doi: 10.1073/pnas.1412075111.

[4] Andrej Fischer, Ignacio Vázquez-García, and Ville Mustonen. The value of monitoring to control evolving populations. *Proceedings of the National Academy of Sciences*, 112(4):1007–1012, 2015. ISSN 0027-8424. doi: 10.1073/pnas.1409403112.

[5] Yoram Louzoun, Chuan Xue, Gregory B. Lesinski, and Avner Friedman. A mathematical model for pancreatic cancer growth and treatments. *Journal of Theoretical Biology*, 351:74–82, 2014. ISSN 00225193. doi: 10.1016/j.jtbi.2014.02.028.

[6] Franziska Michor and Kathryn Beal. Improving Cancer Treatment via Mathematical Modeling: Surmounting the Challenges Is Worth the Effort. *Cell*, 163(5):1059–1063, 2015. ISSN 10974172. doi: 10.1016/j.cell.2015.11.002.

[7] Jingsong Zhang, Jessica J. Cunningham, Joel S. Brown, and Robert A. Gatenby. Integrating evolutionary dynamics into treatment of metastatic castrate-resistant prostate cancer. *Nature Communications*, 8(1):1–10, 2017. ISSN 20411723. doi: 10.1038/s41467-017-01968-5.

[8] Boyang Zhao, Michael T. Hemann, and Douglas A. Lauffenburger. Modeling tumor clonal evolution for drug combinations design. *Trends in Cancer*, 2(3):144–158, mar 2016. ISSN 24058033. doi: 10.1016/j.trecan.2016.02.001.

[9] D. R. Cox. Regression Models and Life-Tables. *Journal of the Royal Statistical Society. Series B, Methodological*, 34(2):187–220, 1972. ISSN 0035-9246. doi: 10.1111/j.2517-6161.1972. tb00899.x.

[10] Artur César Fassoni, Ingo Roeder, and Ingmar Glauche. To Cure or Not to Cure : Consequences of Immunological Interactions in CML Treatment. *Bulletin of Mathematical Biology*, (88881), 2019. ISSN 1522-9602. doi: 10.1007/s11538-019-00608-x.

[11] Christophe Letellier, Sourav Kumar Sasmal, Clément Draghi, Fabrice Denis, and Dibakar Ghosh. A chemotherapy combined with an anti-angiogenic drug applied to a cancer model including angiogenesis. *Chaos, Solitons and Fractals*, 99:297–311, 2017. ISSN 09600779. doi: 10.1016/j.chaos.2017.04.013.

[12] S. T. R. Pinho, F. S. Bacelar, R. F. S. Andrade, and H. I. Freedman. A mathematical model for the effect of anti-angiogenic therapy in the treatment of cancer tumours by chemotherapy. *Nonlinear Analysis: Real World Applications*, 14(1):815–828, 2013. ISSN 14681218. doi: 10.1016/j.nonrwa.2012.07.034.

[13] Sirin Yonucu, Defne Yılmaz, Colin Phipps, Mehmet Burcin Unlu, and Mohammad Kohandel. Quantifying the effects of antiangiogenic and chemotherapy drug combinations on drug delivery and treatment efficacy. *PLoS Computational Biology*, 13(9):1–17, 2017. ISSN 15537358. doi: 10.1371/journal.pcbi.1005724.

[14] Stefano Avanzini and Tibor Antal. Cancer recurrence times from a branching process model. *PLoS Computational Biology*, 15(11):1–30, 2019. ISSN 15537358. doi: 10.1371/journal.pcbi. 1007423.

[15] Emilia Kozłowska, Anniina Färkkilä, Tuulia Vallius, Olli Carpén, Jukka Kemppainen, Seija Grénman, Rainer Lehtonen, Johanna Hynninen, Sakari Hietanen, and Sampsa Hautaniemi. Mathematical modeling predicts response to chemotherapy and drug combinations in ovarian cancer. *Cancer Research*, 78(14):4036–4044, jul 2018. ISSN 15387445. doi: 10.1158/ 0008-5472.CAN-17-3746.

[16] Xiaoran Lai, Oliver M. Geier, Thomas Fleischer, Øystein Garred, Elin Borgen, Simon W. Funke, Surendra Kumar, Marie E. Rognes, Therese Seierstad, Anne-Lise Børresen-Dale, Vessela N. Kristensen, Olav Engebråten, Alvaro Köhn-Luque, and Arnoldo Frigessi. Towards personalized computer simulation of breast cancer treatment : a multi-scale pharmacokinetic and pharmacodynamic model informed by multi-type patient data. *Cancer research*, 2019. doi: 10.1158/0008-5472.CAN-18-1804.

[17] Tomás Alarcón, Markus R. Owen, Helen M. Byrne, and Philip K. Maini. Multiscale modelling of tumour growth and therapy: The influence of vessel normalisation on chemotherapy. *Computational and Mathematical Methods in Medicine*, 7(2-3):85–119, 2006. ISSN 1748670X. doi: 10.1080/10273660600968994.

[18] N. L. Komarova, J. A. Burger, and D. Wodarz. Evolution of ibrutinib resistance in chronic lymphocytic leukemia (CLL). *Proceedings of the National Academy of Sciences*, 111(38):13906– 13911, 2014. ISSN 0027-8424. doi: 10.1073/pnas.1409362111.

[19] Daniel S. Chen and Ira Mellman. Oncology Meets Immunology: The Cancer-Immunity Cycle. *Immunity*, 39(1):1–10, jul 2013. ISSN 10747613. doi: 10.1016/j.immuni.2013.07.012.

[20] Thomas A. Ferguson, Jayoung Choi, and Douglas R. Green. Armed response: How dying cells influence T-cell functions. *Immunological Reviews*, 241(1):77–88, 2011. ISSN 01052896. doi: 10.1111/j.1600-065X.2011.01006.x.

[21] Jingyi Zhou, Gangyang Wang, Yinze Chen, Hongxia Wang, Yingqi Hua, and Zhengdong Cai. Immunogenic cell death in cancer therapy: Present and emerging inducers. *Journal of Cellular and Molecular Medicine*, 23(8):4854–4865, 2019. ISSN 1582-1838. doi: 10.1111/jcmm.14356.

[22] Daniel S. Chen, Bryan A. Irving, and F. Stephen Hodi. Molecular pathways: Next-generation immunotherapy-inhibiting programmed death-ligand 1 and programmed death-1. *Clinical Cancer Research*, 18(24):6580–6587, 2012. ISSN 10780432. doi: 10.1158/1078-0432. CCR-12-1362.

[23] Drew M. Pardoll. The blockade of immune checkpoints in cancer immunotherapy. *Nature Reviews Cancer*, 12(4):252–264, 2012. ISSN 1474175X. doi: 10.1038/nrc3239.

[24] F. Stephen Hodi, Steven J. O'Day, David F. McDermott, Robert W. Weber, Jeffrey A. Sosman, John B. Haanen, Rene Gonzalez, Caroline Robert, Dirk Schadendorf, Jessica C. Hassel, Wallace Akerley, Alfons J. M. van den Eertwegh, Jose Lutzky, Paul Lorigan, Julia M. Vaubel, Gerald P. Linette, David Hogg, Christian H. Ottensmeier, Celeste Lebbé, Christian Peschel, Ian Quirt, Joseph I. Clark, Jedd D. Wolchok, Jeffrey S. Weber, Jason Tian, Michael J. Yellin, Geoffrey M. Nichol, Axel Hoos, and Walter J. Urba. Improved Survival with Ipilimumab in Patients with Metastatic Melanoma. *New England Journal of Medicine*, 363(8):711–723, aug 2010. ISSN 0028-4793. doi: 10.1056/nejmoa1003466.

[25] Greg T. Motz and George Coukos. Deciphering and Reversing Tumor Immune Suppression. *Immunity*, 39(1):61–73, 2013. ISSN 10747613. doi: 10.1016/j.immuni.2013.07.005.

[26] Chengwen Liu, Weiyi Peng, Chunyu Xu, Yanyan Lou, Minying Zhang, Jennifer A. Wargo, Jie Qing Chen, Haiyan S. Li, Stephanie S. Watowich, Yan Yang, Dennie Tompers Frederick,

Zachary A. Cooper, Rina M. Mbofung, Mayra Whittington, Keith T. Flaherty, Scott E. Woodman, Michael A. Davies, Laszlo G. Radvanyi, Willem W. Overwijk, Gregory Lizée, and Patrick Hwu. BRAF inhibition increases tumor infiltration by T cells and enhances the antitumor activity of adoptive immunotherapy in mice. *Clinical Cancer Research*, 19(2):393–403, 2013. ISSN 10780432. doi: 10.1158/1078-0432.CCR-12-1626.

[27] Carl H. June, Roddy S. O'Connor, Omkar U. Kawalekar, Saba Ghassemi, and Michael C. Milone. CAR T cell immunotherapy for human cancer. *Science*, 359(6382):1361–1365, 2018. ISSN 10959203. doi: 10.1126/science.aar6711.

[28] Young Kwang Chae, Ayush Arya, Wade Iams, Marcelo R. Cruz, Sunandana Chandra, Jaehyuk Choi, and Francis Giles. Current landscape and future of dual anti-CTLA4 and PD-1/PD-L1 blockade immunotherapy in cancer; lessons learned from clinical trials with melanoma and non-small cell lung cancer (NSCLC). *Journal for ImmunoTherapy of Cancer*, 6(1):39, dec 2018. ISSN 2051-1426. doi: 10.1186/s40425-018-0349-3.

[29] Dev Karan and Peter Van Veldhuizen. Combination immunotherapy with prostate GVAX and ipilimumab: safety and toxicity. *Immunotherapy*, 4(6):577–580, jun 2012. ISSN 1750-743X. doi: 10.2217/imt.12.53.

[30] Ravi A. Madan, Mahsa Mohebtash, Philip M. Arlen, Matteo Vergati, Myrna Rauckhorst, Seth M. Steinberg, Kwong Y. Tsang, Diane J. Poole, Howard L. Parnes, John J. Wright, William L. Dahut, Jeffrey Schlom, and James L. Gulley. Ipilimumab and a poxviral vaccine targeting prostate-specific antigen in metastatic castration-resistant prostate cancer: A phase 1 dose-escalation trial. *The Lancet Oncology*, 13(5):501–508, 2012. ISSN 14702045. doi: 10.1016/S1470-2045(12)70006-2.

[31] Jedd D. Wolchok, Harriet Kluger, Margaret K. Callahan, Michael A. Postow, Naiyer A. Rizvi, Alexander M. Lesokhin, Neil H. Segal, Charlotte E. Ariyan, Ruth-Ann Gordon, Kathleen Reed, Matthew M. Burke, Anne Caldwell, Stephanie A. Kronenberg, Blessing U. Agunwamba, Xiaoling Zhang, Israel Lowy, Hector David Inzunza, William Feely, Christine E. Horak, Quan Hong, Alan J. Korman, Jon M. Wigginton, Ashok Gupta, and Mario Sznol. Nivolumab plus Ipilimumab in Advanced Melanoma. *New England Journal of Medicine*, 369(2):122–133, 2013. ISSN 0028-4793. doi: 10.1056/nejmoa1302369.

[32] Vikas Malhotra and Michael C. Perry. Classical chemotherapy: mechanisms, toxicities and the therapeutic window. *Cancer biology & therapy*, 2(4 Suppl 1):4–6, 2003. ISSN 15384047. doi: 10.4161/cbt.199.

[33] Kabir A. Khan and Roy Bicknell. Anti-angiogenic alternatives to VEGF blockade. *Clinical and Experimental Metastasis*, 33(2):197–210, 2016. ISSN 15737276. doi: 10.1007/s10585-015-9769-3.

[34] Mehdi Rajabi and Shaker A. Mousa. The role of angiogenesis in cancer treatment. *Biomedicines*, 5(2), 2017. ISSN 22279059. doi: 10.3390/biomedicines5020034.

[35] Rakesh R. Ramjiawan, Arjan W. Griffioen, and Dan G. Duda. Anti-angiogenesis for cancer revisited: Is there a role for combinations with immunotherapy? *Angiogenesis*, 20(2):185–204, 2017. ISSN 15737209. doi: 10.1007/s10456-017-9552-y.

[36] Hal L. Smith and Paul E. Waltman. *The theory of the chemostat : dynamics of microbial competition*. Cambridge University Press, 1995. ISBN 0521470277.

[37] Peter Tóth and János Érdi. *Mathematical Models of Chemical Reactions: Theory and Applications of Deterministic and Stochastic Models*. Manchester University Press, 1989. ISBN ISBN 978-0-7190-2208-1.

[38] I. F. Tannock. The relation between cell proliferation and the vascular system in a transplanted mouse mammary tumour. *British Journal of Cancer*, 22(2):258–273, 1968. ISSN 15321827. doi: 10.1038/bjc.1968.34.

[39] Rudolf Gesztelyi, Judit Zsuga, Adam Kemeny-Beke, Balazs Varga, Bela Juhasz, and Arpad Tosaki. The Hill equation and the origin of quantitative pharmacology. *Archive for History of Exact Sciences*, 66(4):427–438, 2012. ISSN 00039519. doi: 10.1007/s00407-012-0098-5.

[40] Greg T. Motz and George Coukos. Deciphering and Reversing Tumor Immune Suppression. *Immunity*, 39(1):61–73, 2013. ISSN 10747613. doi: 10.1016/j.immuni.2013.07.005.

[41] Mary L. Disis. Immune regulation of cancer. *Journal of Clinical Oncology*, 28(29):4531–4538, 2010. ISSN 0732183X. doi: 10.1200/JCO.2009.27.2146.

[42] Julio A. Aguirre-Ghiso. Models, mechanisms and clinical evidence for cancer dormancy. *Nature Reviews Cancer*, 7(11):834–846, 2007. ISSN 1474175X. doi: 10.1038/nrc2256.

[43] Liliana Ossowski and Julio A. Aguirre-Ghiso. Dormancy of metastatic melanoma. *Pigment Cell and Melanoma Research*, 23(1):41–56, 2010. ISSN 17551471. doi: 10.1111/j.1755-148X.2009.00647.x.

[44] Robert D. Schreiber, Lloyd J. Old, and Mark J. Smyth. Cancer immunoediting: Integrating immunity's roles in cancer suppression and promotion. *Science*, 331(6024):1565–1570, 2011. ISSN 00368075. doi: 10.1126/science.1203486.

[45] Daniela Senft and Ze'ev A. Ronai. Immunogenic, cellular, and angiogenic drivers of tumor dormancy-a melanoma view. *Pigment Cell and Melanoma Research*, 29(1):27–42, 2016. ISSN 1755148X. doi: 10.1111/pcmr.12432.

[46] Suzanne L. Topalian, Mario Sznol, David F. McDermott, Harriet M. Kluger, Richard D. Carvajal, William H. Sharfman, Julie R. Brahmer, Donald P. Lawrence, Michael B. Atkins, John D. Powderly, Philip D. Leming, Evan J. Lipson, Igor Puzanov, David C. Smith, Janis M. Taube, Jon M. Wigginton, Georgia D. Kollia, Ashok Gupta, Drew M. Pardoll, Jeffrey A. Sosman, and F. Stephen Hodi. Survival, durable tumor remission, and long-term safety in patients with advanced melanoma receiving nivolumab. *Journal of Clinical Oncology*, 32(10):1020–1030, 2014. ISSN 15277755. doi: 10.1200/JCO.2013.53.0105.

[47] Z. J. Wolner, A. A. Marghoob, M. P. Pulitzer, M. A. Postow, and M. A. Marchetti. A case report of disappearing pigmented skin lesions associated with pembrolizumab treatment for metastatic melanoma. *British Journal of Dermatology*, 178(1):265–269, 2018. ISSN 13652133. doi: 10.1111/bjd.15354.

[48] J. Hamish E. Laing, George D. Wilson, and Christine A. Martindale. Proliferation rates in human malignant melanoma. *Melanoma Research*, 13(3):271–277, 2003. ISSN 0960-8931. doi: 10.1097/00008390-200306000-00008.

[49] Ingunn Tufto and Einar K. Rofstad. Interstitial Fluid Pressure, Fraction of Necrotic Tumor Tissue, and Tumor Cell Density in Human Melanoma Xenografts. *Acta Oncologica*, 37(3):291–297, jan 1998. ISSN 0284-186X. doi: 10.1080/028418698429603.

[50] Gavin P. Dunn, Lloyd J. Old, and Robert D. Schreiber. The immunobiology of cancer immunosurveillance and immunoediting, 2004. ISSN 10747613.

[51] Jake S. O'Donnell, Michele W. L. Teng, and Mark J. Smyth. Cancer immunoediting and resistance to T cell-based immunotherapy. *Nature Reviews Clinical Oncology*, 16(3):151–167, 2019. ISSN 17594782. doi: 10.1038/s41571-018-0142-8.

[52] Alexander C. Huang, Robert J. Orlowski, Xiaowei Xu, Rosemarie Mick, Sangeeth M. George, Patrick K. Yan, Sasikanth Manne, Adam A. Kraya, Bradley Wubbenhorst, Liza Dorfman, Kurt D'Andrea, Brandon M. Wenz, Shujing Liu, Lakshmi Chilukuri, Andrew Kozlov, Mary Carberry, Lydia Giles, Melanie W. Kier, Felix Quagliarello, Suzanne McGettigan, Kristin Kreider, Lakshmanan Annamalai, Qing Zhao, Robin Mogg, Wei Xu, Wendy M. Blumenschein, Jennifer H. Yearley, Gerald P. Linette, Ravi K. Amaravadi, Lynn M. Schuchter, Ramin S. Herati, Bertram Bengsch, Katherine L. Nathanson, Michael D. Farwell, Giorgos C. Karakousis, E. John Wherry, and Tara C. Mitchell. A single dose of neoadjuvant PD-1 blockade predicts clinical outcomes in resectable melanoma. *Nature Medicine*, 25(3):454–461, 2019. ISSN 1546170X. doi: 10.1038/s41591-019-0357-y.

[53] Hirokazu Tokuyasu, Soichiro Ishikawa, Hiromitsu Sakai, Tomoyuki Ikeuchi, and Hiroshi Miura. Single pembrolizumab treatment causing profound durable response in a patient with pulmonary pleomorphic carcinoma. *Respiratory Medicine Case Reports*, 28(June):26–30, 2019. ISSN 22130071. doi: 10.1016/j.rmcr.2019.100879.

[54] Shaoming Zhu, Tian Zhang, Lei Zheng, Hongtao Liu, Wenru Song, Delong Liu, Zihai Li, and Chong xian Pan. Combination strategies to maximize the benefits of cancer immunotherapy. *Journal of Hematology and Oncology*, 14(1):1–33, 2021. ISSN 17568722. doi: 10.1186/s13045-021-01164-5.

[55] Mikko Heino and Ilkka Hanski. Evolution of migration rate in a spatially realistic metapopulation model. *American Naturalist*, 157(5):495–511, 2001. ISSN 00030147. doi: 10.1086/319927.

[56] Tuomas Nurmi and Kalle Parvinen. On the evolution of specialization with a mechanistic underpinning in structured metapopulations. *Theoretical Population Biology*, 73(2):222–243, 2008. ISSN 00405809. doi: 10.1016/j.tpb.2007.12.002.

[57] Kalle Parvinen. Evolution of dispersal in a structured metapopulation model in discrete time. *Bulletin of Mathematical Biology*, 68(3):655–678, 2006. ISSN 00928240. doi: 10.1007/s11538-005-9040-1.

[58] Kalle Parvinen and Johan A. J. Metz. A novel fitness proxy in structured locally finite metapopulations with diploid genetics, with an application to dispersal evolution. *Theoretical Population Biology*, 73(4):517–528, 2008. ISSN 00405809. doi: 10.1016/j.tpb.2008.01.002.

[59] Kalle Parvinen. Adaptive Dynamics of Altruistic Cooperation in a Metapopulation: Evolutionary Emergence of Cooperators and Defectors or Evolutionary Suicide? *Bulletin of Mathematical Biology*, 73(11):2605–2626, 2011. ISSN 00928240. doi: 10.1007/s11538-011-9638-4.

[60] Kalle Parvinen, Hisashi Ohtsuki, and Joe Yuichiro Wakano. Spatial heterogeneity and evolution of fecundity-affecting traits. *Journal of Theoretical Biology*, 454:190–204, 2018. ISSN 10958541. doi: 10.1016/j.jtbi.2018.06.005.

[61] Kalle Parvinen, Hisashi Ohtsuki, and Joe Yuichiro Wakano. Evolution of dispersal in a spatially heterogeneous population with finite patch sizes. *Proceedings of the National Academy of Sciences of the United States of America*, 117(13):7290–7295, 2020. ISSN 10916490. doi: 10.1073/pnas.1915881117.

[62] Helene C. Weigang and Éva Kisdi. Evolution of dispersal under a fecundity-dispersal trade-off. *Journal of Theoretical Biology*, 371:145–153, 2015. ISSN 10958541. doi: 10.1016/j.jtbi.2015.02.013.

[63] Åke Brännström, Jacob Johansson, and Niels von Festenberg. The Hitchhiker's guide to adaptive dynamics. *Games*, 4(3):304–328, 2013. ISSN 20734336. doi: 10.3390/g4030304.

[64] Odo Diekmann. A beginner's guide to adaptive dynamics. *Banach Center Publications*, 63: 47–86, 2003. ISSN 0137-6934. doi: 10.4064/bc63-0-2.

[65] S. A. H. Geritz, É Kisdi, G. Meszéna, and J. A. J. Metz. Evolutionarily singular strategies and the adaptive growth and branching of the evolutionary tree. *Evolutionary Ecology*, 12(1):35–57, 1998. ISSN 02697653. doi: 10.1023/A:1006554906681.

[66] Judah Folkman. How Is Blood Vessel Growth Regulated in Normal and Neoplastic Tissue?- G. H. A. Clowes Memorial Award Lecture. *Cancer Research*, 46:467–473, 1986.

[67] Lance Allen Liotta, Jerome Kleinerman, and Gerald M. Saidel. Quantitative Relationships of Intravascular Tumor Cells, Tumor Vessels, and Pulmonary Metastases following Tumor Implantation. *Cancer Research*, 34(5):997–1004, 1974. ISSN 15387445.

[68] Naoyo Nishida, Hirohisa Yano, Takashi Nishida, Toshiharu Kamura, and Masamichi Kojiro. Angiogenesis in cancer. *Vascular Health and Risk Management*, 2(3):213–219, 2006. ISSN 11766344. doi: 10.2147/vhrm.2006.2.3.213.

[69] Yutaka Takahashi, Yasuhiko Kitadai, Corazon D. Bucana, Lee M. Ellis, Yutaka Takahashi, Lee M. Ellis, and Karen R. Cleary. Expression of Vascular Endothelial Growth Factor and Its Receptor, KDR, Correlates with Vascularity, Metastasis, and Proliferation of Human Colon Cancer. *Cancer Research*, 55(18):3969–3972, 1995. ISSN 15387445.

[70] Gabriele Bergers and Douglas Hanahan. Modes of resistance to anti-angiogenic therapy. *Nature Reviews Cancer*, 8(8):592–603, aug 2008. ISSN 1474-175X. doi: 10.1038/nrc2442.

[71] John D. Nagy and Dieter Armbruster. Evolution of uncontrolled proliferation and the angiogenic switch in cancer. *Mathematical Biosciences and Engineering*, 9(4):843–876, oct 2012. ISSN 1551-0018. doi: 10.3934/mbe.2012.9.843.

[72] Rui D. M. Travasso, Eugenia Corvera Poiré, Mario Castro, Juan Carlos Rodrguez-Manzaneque, and A. Hernández-Machado. Tumor angiogenesis and vascular patterning: A mathematical model. *PLoS ONE*, 6(5):1–10, 2011. ISSN 19326203. doi: 10.1371/journal.pone.0019989.

[73] Jiangping Xu, Guillermo Vilanova, and Hector Gomez. A mathematical model coupling tumor growth and angiogenesis. *PLoS ONE*, 11(2):1–20, 2016. ISSN 19326203. doi: 10.1371/journal.pone.0149422.

[74] Luke Olsen, Jonathan A. Sherratt, Philip K. Maini, and Frank Arnold. A mathematical model for the capillary endothelial cell-extracellular matrix interactions in wound-healing angiogenesis. *IMA Journal of Mathathics Applied in Medicine and Biology*, 14(4):261–281, 1997. ISSN 02650746. doi: 10.1093/imammb/14.4.261.

[75] Richard C. Schugart, Avner Friedman, Rui Zhao, and Chandan K. Sen. Wound angiogenesis as a function of tissue oxygen tension: A mathematical model. *Proceedings of the National Academy of Sciences of the United States of America*, 105(7):2628–2633, 2008. ISSN 00278424. doi: 10.1073/pnas.0711642105.

[76] Diane R. Bielenberg and Bruce R. Zetter. The Contribution of Angiogenesis to the Process of Metastasis. *Cancer Journal (United States)*, 21(4):267–273, 2015. ISSN 1540336X. doi: 10.1097/PPO.0000000000000138.

[77] Dietmar W. Siemann. The Unique Characteristics of Tumor Vasculature and Preclinical Evidence for its Selective Disruption by Tumor-Vascular Disrupting Agents. *Cancer Treatment Reviews*, 37(1):63–74, 2011. doi: 0.1016/j.ctrv.2010.05.001.

[78] Fabienne Baffert, Gavin Thurston, Michael Rochon-Duck, Tom Le, Rolf Brekken, and Donald M. McDonald. Age-Related Changes in Vascular Endothelial Growth Factor Dependency and Angiopoietin-1-Induced Plasticity of Adult Blood Vessels. *Circulation Research*, 94(7):984–992, 2004. ISSN 00097330. doi: 10.1161/01.RES.0000125295.43813.1F.

[79] Michael S. Gee, William N. Procopio, Sosina Makonnen, Michael D. Feldman, Newman M. Yeilding, and William M. F. Lee. Tumor vessel development and maturation impose limits on the effectiveness of anti-vascular therapy. *American Journal of Pathology*, 162(1):183–193, 2003. ISSN 00029440. doi: 10.1016/S0002-9440(10)63809-6.

[80] Sajani S. Lakka and Jasti S. Rao. Antiangiogenic therapy in brain tumors. *Expert Review Neurotherapeutics*, 8(10):1457–1473, 2008. doi: 10.1586/14737175.8.10.1457.

[81] Domenico Ribatti, Tiziana Annese, Simona Ruggieri, Roberto Tamma, and Enrico Crivellato. Limitations of Anti-Angiogenic Treatment of Tumors. *Translational Oncology*, 12(7):981–986, 2019. ISSN 19365233. doi: 10.1016/j.tranon.2019.04.022.

[82] Kabir A. Khan and Robert S. Kerbel. Improving immunotherapy outcomes with anti-angiogenic treatments and vice versa. *Nature Reviews Clinical Oncology*, 15(5):310–324, 2018. ISSN 17594782. doi: 10.1038/nrclinonc.2018.9.

[83] Won Suk Lee, Hannah Yang, Hong Jae Chon, and Chan Kim. Combination of anti-angiogenic therapy and immune checkpoint blockade normalizes vascular-immune crosstalk to potentiate cancer immunity. *Experimental and Molecular Medicine*, 52(9):1475–1485, 2020. ISSN 20926413. doi: 10.1038/s12276-020-00500-y.

[84] Francesca Elice and Francesco Rodeghiero. PL-09 side effects of anti-angiogenic drugs. *Thrombosis Research*, 129(SUPPL. 1):S50–S53, 2012. ISSN 00493848. doi: 10.1016/S0049-3848(12)70016-6.

[85] Muhammad Wasif Saif, Aymen Elfiky, and Ronald R. Salem. Gastrointestinal perforation due to bevacizumab in colorectal cancer. *Annals of Surgical Oncology*, 14(6):1860–1869, 2007. ISSN 10689265. doi: 10.1245/s10434-006-9337-9.

[86] Liang Qiao and Geofrrey C. Farrell. The effects of cell density, attachment substratum and dexamethasone on spontaneous apoptosis of rat hepatocytes in primary culture. *In Vitro Cellular and Developmental Biology - Animal*, 35(7):417–424, 1999. ISSN 10712690. doi: 10.1007/s11626-999-0117-2.

[87] Dorothy H. Rowe, Jianzhong Huang, Mark L. Kayton, Richard Thompson, Andrea Troxel, Kathleen M. O'Toole, Darrell Yamashiro, Charles J.H. Stolar, and Jessica J. Kandel. Anti-

VEGF antibody suppresses primary tumor growth and metastasis in an experimental model of Wilms' tumor. *Journal of Pediatric Surgery*, 35(1):30–33, 2000. ISSN 00223468. doi: 10.1016/S0022-3468(00)80008-1.

[88] Robert S. Warren, Hui Yuan, Mary R. Matli, Nancy A. Gillett, and Napoleone Ferrara. Regulation by vascular endothelial growth factor of human colon cancer tumorigenesis in a mouse model of experimental liver metastasis. *Journal of Clinical Investigation*, 95(4):1789–1797, 1995. ISSN 00219738. doi: 10.1172/JCI117857.

[89] J. A. J. Metz, R. M. Nisbet, and S. A. H. Geritz. How should we define 'fitness' for general ecological scenarios? *Trends in Ecology & Evolution*, 7(6):198–202, jun 1992. ISSN 01695347. doi: 10.1016/0169-5347(92)90073-K.

[90] J. A. J. Metz and M. Gyllenberg. How should we define fitness in structured metapopulation models? Including an application to the calculation of evolutionarily stable dispersal strategies. *Proceedings of the Royal Society B: Biological Sciences*, 268(1466):499–508, 2001. ISSN 14712970. doi: 10.1098/rspb.2000.1373.

[91] John G. Kemeny and J. Laurie Snell. *Finite Markov chains*. Princeton, 1960.

[92] W. D. Hamilton. The genetical evolution of social behaviour. I. *Journal of Theoretical Biology*, 7:1–16, 7 1964. ISSN 00225193. doi: 10.1016/0022-5193(64)90038-4.

[93] Robert Tibshirani. The lasso method for variable selection in the cox model. *Statistics in Medicine*, 16(4):385–395, 1997. ISSN 02776715. doi: 10.1002/(SICI)1097-0258(19970228)16: 4⟨385::AID-SIM380⟩3.0.CO;2-3.

[94] Noah Simon, Jerome Friedman, Trevor Hastie, and Rob Tibshirani. Regularization paths for Cox's proportional hazards model via coordinate descent. *Journal of Statistical Software*, 39(5): 1–13, 2011. ISSN 15487660. doi: 10.18637/jss.v039.i05.

[95] Justin Guinney, Tao Wang, Teemu D. Laajala, Kimberly Kanigel Winner, J. Christopher Bare, Elias Chaibub Neto, Suleiman A. Khan, Gopal Peddinti, Antti Airola, Tapio Pahikkala, Tuomas Mirtti, Thomas Yu, Brian M. Bot, Liji Shen, Kald Abdallah, Thea Norman, Stephen Friend, Gustavo Stolovitzky, Howard Soule, Christopher J. Sweeney, Charles J. Ryan, Howard I. Scher, Oliver Sartor, Yang Xie, Tero Aittokallio, Fang Liz Zhou, and James C. Costello. Prediction of overall survival for patients with metastatic castration-resistant prostate cancer: development of a prognostic model through a crowdsourced challenge with open clinical trial data. *The Lancet Oncology*, 18(1):132–142, 2017. ISSN 14745488. doi: 10.1016/S1470-2045(16)30560-5.

[96] Andrew J. Armstrong, Elizabeth S. Garrett-Mayer, Yi Chun Ou Yang, Ronald De Wit, Ian F. Tannock, and Mario Eisenberger. A contemporary prognostic nomogram for men with hormone-refractory metastatic prostate cancer: A TAX327 study analysis. *Clinical Cancer Research*, 13 (21):6396–6403, 2007. ISSN 10780432. doi: 10.1158/1078-0432.CCR-07-1036.

[97] Carine A Bellera, Gaëtan MacGrogan, Marc Debled, Christine Tunon de Lara, Véronique Brouste, and Simone Mathoulin-Pélissier. Variables with time-varying effects and the cox model: Some statistical concepts illustrated with a prognostic factor study in breast cancer. *BMC Medical Research Methodology*, 10:20, 12 2010. ISSN 1471-2288. doi: 10.1186/1471-2288-10-20.

[98] Jiadong Chu, Na Sun, Wei Hu, Xuanli Chen, Nengjun Yi, and Yueping Shen. The application of bayesian methods in cancer prognosis and prediction. *Cancer Genomics - Proteomics*, 19:1–11, 12 2022. ISSN 1109-6535. doi: 10.21873/cgp.20298.

[99] Susan Halabi, Chen Yen Lin, W. Kevin Kelly, Karim Fizazi, Judd W. Moul, Ellen B. Kaplan, Michael J. Morris, and Eric J. Small. Updated prognostic model for predicting overall survival in first-line chemotherapy for patients with metastatic castration-resistant prostate cancer. *Journal of Clinical Oncology*, 32(7):671–677, 2014. ISSN 15277755. doi: 10.1200/JCO.2013.52.3696.

[100] Richard Meier, Stefan Graw, Joseph Usset, Rama Raghavan, Junqiang Dai, Prabhakar Chalise, Shellie Ellis, Brooke Fridley, and Devin Koestler. An ensemble-based Cox proportional hazards regression framework for predicting survival in metastatic castration-resistant prostate cancer (mCRPC) patients. *F1000Research*, 5(0):1–16, 2016. ISSN 1759796X. doi: 10.12688/ f1000research.8226.1.

[101] Hideyuki Shimizu and Keiichi I. Nakayama. A 23 gene–based molecular prognostic score precisely predicts overall survival of breast cancer patients. *EBioMedicine*, 46:150–159, 8 2019. ISSN 23523964. doi: 10.1016/j.ebiom.2019.07.046.

[102] Wan Zhu, Longxiang Xie, Jianye Han, and Xiangqian Guo. The application of deep learning in cancer prognosis prediction. *Cancers*, 12:603, 3 2020. ISSN 2072-6694. doi: 10.3390/cancers12030603.

[103] Mee Young Park and Trevor Hastie. L1-regularization path algorithm for generalized linear models. *Journal of the Royal Statistical Society. Series B: Statistical Methodology*, 69(4):659–677, 2007. ISSN 13697412. doi: 10.1111/j.1467-9868.2007.00607.x.

[104] Jelle J. Goeman. L1 penalized estimation in the Cox proportional hazards model. *Biometrical Journal*, 52(1):70–84, 2010. ISSN 03233847. doi: 10.1002/bimj.200900028.

[105] Jean-Philippe Chancelier and Michel De Lara. Capra-Convexity, Convex Factorization and Variational Formulations for the ℓ_0 Pseudonorm. *Set-Valued and Variational Analysis*, 30(2):597–619, jun 2022. ISSN 1877-0533. doi: 10.1007/s11228-021-00606-z.

[106] Manlio Gaudioso, E. Gorgone, and J. B. Hiriart-Urruty. Feature selection in SVM via polyhedral k-norm. *Optimization Letters*, 14(1):19–36, 2020. ISSN 18624480. doi: 10.1007/s11590-019-01482-1.

[107] Jun-ya Gotoh, Akiko Takeda, and Katsuya Tono. *DC formulations and algorithms for sparse optimization problems*, volume 169. Springer Berlin Heidelberg, 2018. ISBN 1010701711. doi: 10.1007/s10107-017-1181-0.

[108] B. K. Natarajan. Sparse approximate solutions to linear systems. *SIAM Journal on Computing*, 24(2):227–234, 1995. ISSN 00975397. doi: 10.1137/S0097539792240406.

[109] Shai Shalev-Shwartz, Nathan Srebro, and Tong Zhang. Trading Accuracy for Sparsity in Optimization Problems with Sparsity Constraints. *SIAM Journal on Optimization*, 20(6):2807–2832, jan 2010. ISSN 1052-6234. doi: 10.1137/090759574.

[110] Wenchuan Guo, Shujie Ma, and Zhenqiu Liu. l0ara. URL `https://cran.r-project.org/package=l0ara`.

[111] Hussein Hazimeh and Rahul Mazumder. Fast best subset selection: Coordinate descent and local combinatorial optimization algorithms. *Operations Research*, 68(5):1517–1537, 2020. ISSN 15265463. doi: 10.1287/opre.2019.1919.

[112] Xiang Li, Shanghong Xie, Donglin Zeng, and Yuanjia Wang. Efficient ℓ_0-norm feature selection based on augmented and penalized minimization. *Statistics in Medicine*, 37(3):473–486, 2018. ISSN 10970258. doi: 10.1002/sim.7526.

[113] Kaisa Joki and Adil M. Bagirov. Bundle methods for nonsmooth DC optimization. In Adil M. Bagirov, Manlio Gaudioso, Napsu Karmitsa, Marko M. Mäkelä, and Sona Taheri, editors, *Numerical Nonsmooth Optimization: State of the Art Algorithms*, pages 263–296. Springer International Publishing, Cham, 2020. ISBN 9783030349103. doi: 10.1007/978-3-030-34910-3_8.

[114] Kaisa Joki, Adil M. Bagirov, Napsu Karmitsa, Marko M. Mäkelä, and Sona Taheri. Double Bundle Method for finding Clarke Stationary Points in Nonsmooth DC Programming. *SIAM Journal on Optimization*, 28(2):1892–1919, jan 2018. ISSN 1052-6234. doi: 10.1137/16M1115733.

[115] M. Haarala, K. Miettinen, and M. M. Mäkelä. New limited memory bundle method for large-scale nonsmooth optimization. *Optimization Methods and Software*, 19(6):673–692, 2004.

[116] Napsu Haarala, Kaisa Miettinen, and Marko M. Mäkelä. Globally convergent limited memory bundle method for large-scale nonsmooth optimization. *Mathematical Programming*, 109(1):181–205, 2007.

[117] Nicolas Mottet, Joaquim Bellmunt, Michel Bolla, Erik Briers, Marcus G. Cumberbatch, Maria De Santis, Nicola Fossati, Tobias Gross, Ann M. Henry, Steven Joniau, Thomas B. Lam, Malcolm D. Mason, Vsevolod B. Matveev, Paul C. Moldovan, Roderick C.N. van den Bergh, Thomas Van den Broeck, Henk G. van der Poel, Theo H. van der Kwast, Olivier Rouvière, Ivo G. Schoots, Thomas Wiegel, and Philip Cornford. EAU-ESTRO-SIOG Guidelines on Prostate Cancer. Part 1: Screening, Diagnosis, and Local Treatment with Curative Intent. *European Urology*, 71(4):618–629, 2017. ISSN 18737560. doi: 10.1016/j.eururo.2016.08.003.

[118] Frank E. Harrell Jr, Robert M. Califf, David B. Pryor, Kerry L. Lee, and Robert A. Rosati. Evaluating the yield of medical tests. *JAMA*, 247(18):2543–2546, 1982. doi: 10.1001/jama. 1982.03320430047030.

[119] Hung Hung and Chin-Tsang Chiang. Estimation methods for time-dependent AUC models with survival data. *Canadian Journal of Statistics*, 38(1):8–26, 2010. ISSN 03195724. doi: 10.1002/ cjs.10046.

[120] Daniel P. Petrylak, Nicholas J. Vogelzang, Nikolay Budnik, Pawel Jan Wiechno, Cora N. Sternberg, Kevin Doner, Joaquim Bellmunt, John M. Burke, Maria Ochoa de Olza, Ananya Choudhury, Juergen E. Gschwend, Evgeny Kopyltsov, Aude Flechon, Nicolas Van As, Nadine Houede, Debora Barton, Abderrahim Fandi, Ulf Jungnelius, Shaoyi Li, Ronald de Wit, and Karim Fizazi. Docetaxel and prednisone with or without lenalidomide in chemotherapy-naive patients with metastatic castration-resistant prostate cancer (MAINSAIL): A randomised, double-blind, placebo-controlled phase 3 trial. *The Lancet Oncology*, 16(4):417–425, 2015. ISSN 14745488. doi: 10.1016/S1470-2045(15)70025-2.

[121] Ian F. Tannock, Karim Fizazi, Sergey Ivanov, Camilla Thellenberg Karlsson, Aude Fléchon, Iwona Skoneczna, Francisco Orlandi, Gwenaelle Gravis, Vsevolod Matveev, Sevil Bavbek, Thierry Gil, Luciano Viana, Osvaldo Arén, Oleg Karyakin, Tony Elliott, Alison Birtle, Emmanuelle Magherini, Laurence Hatteville, Daniel Petrylak, Bertrand Tombal, and Mark Rosenthal. Aflibercept versus placebo in combination with docetaxel and prednisone for treatment of men with metastatic castration-resistant prostate cancer (VENICE): A phase 3, double-blind randomised trial. *The Lancet Oncology*, 14(8):760–768, 2013. ISSN 14702045. doi: 10.1016/S1470-2045(13)70184-0.

[122] Howard I. Scher, Xiaoyu Jia, Kim Chi, Ronald De Wit, William R. Berry, Peter Albers, Brian Henick, David Waterhouse, Dean J. Ruether, Peter J. Rosen, Anthony A. Meluch, Luke T. Nordquist, Peter M. Venner, Axel Heidenreich, Luis Chu, and Glenn Heller. Randomized, open-label phase III trial of docetaxel plus high-dose calcitriol versus docetaxel plus prednisone for patients with castration-resistant prostate cancer. *Journal of Clinical Oncology*, 29(16):2191–2198, 2011. ISSN 0732183X. doi: 10.1200/JCO.2010.32.8815.

[123] Project Data Sphere. URL https://www.projectdatasphere.org/.

[124] Teemu D. Laajala, Mika Murtojärvi, Arho Virkki, and Tero Aittokallio. EPCR: An R-package for survival and time-to-event prediction in advanced prostate cancer, applied to real-world patient cohorts. *Bioinformatics*, 34(22):3957–3959, 2018. ISSN 14602059. doi: 10.1093/bioinformatics/bty477.

[125] N. E. Breslow. Contribution to the discussion of the paper by D.R. Cox. *Journal of the Royal Statistical Society B*, 34:216–217, 1972.

[126] Stephen P. Boyd and Lieven Vandenberghe. *Convex optimization*. Cambridge University Press, Cambridge ;, 2004. ISBN 0-521-83378-7.

[127] Jorge. Nocedal and Stephen J. Wright. *Numerical optimization*. Springer series in operations research and financial engineering. Springer, New York, 2nd ed. edition, 2006. ISBN 9780387400655. doi: 10.1201/b19115-11.

[128] Willard I. Zangwill. Non-Linear Programming Via Penalty Functions. *Management Science*, 13 (5):344–358, 1967.

[129] Evan J. Lipson, William H. Sharfman, Charles G. Drake, Ira Wollner, Janis M. Taube, Robert A. Anders, Haiying Xu, Sheng Yao, Alice Pons, Lieping Chen, Drew M. Pardoll, Julie R. Brahmer, and Suzanne L. Topalian. Durable cancer regression off-treatment and effective reinduction therapy with an anti-PD-1 antibody. *Clinical Cancer Research*, 19(2):462–468, 2013. ISSN 10780432. doi: 10.1158/1078-0432.CCR-12-2625.

[130] K. L. Eales, K. E. R. Hollinshead, and D. A. Tennant. Hypoxia and metabolic adaptation of cancer cells. *Oncogenesis*, 5(1):e190–e190, 2016. doi: 10.1038/oncsis.2015.50.

[131] Gabriele Grasmann, Ayusi Mondal, and Katharina Leithner. Flexibility and adaptation of cancer cells in a heterogenous metabolic microenvironment. *International Journal of Molecular Sciences*, 22(3):1–19, 2021. ISSN 14220067. doi: 10.3390/ijms22031476.

[132] M. Gerlinger and C. Swanton. How Darwinian models inform therapeutic failure initiated by clonal heterogeneity in cancer medicine. *British Journal of Cancer*, 103(8):1139–1143, 2010. ISSN 15321827. doi: 10.1038/sj.bjc.6605912.

[133] Shahneen Sandhu, Caroline M. Moore, Edmund Chiong, Himisha Beltran, Robert G. Bristow, and Scott G. Williams. Prostate cancer. *The Lancet*, 398(10305):1075–1090, 2021. ISSN 1474547X. doi: 10.1016/S0140-6736(21)00950-8.

[134] Daniel Heinrich, Oyvind Bruland, Theresa A. Guise, Hiroyoshi Suzuki, and Oliver Sartor. Alkaline phosphatase in metastatic castration-resistant prostate cancer: Reassessment of an older biomarker. *Future Oncology*, 14(24):2543–2556, 2018. ISSN 17448301. doi: 10.2217/fon-2018-0087.

[135] William R. Berry, John Laszlo, Edwin Cox, Ann Walker, and David Paulson. Prognostic factors in metastatic and hormonally unresponsive carcinoma of the prostate. *Cancer*, 44(2):763–775, aug 1979. ISSN 0008-543X. doi: 10.1002/1097-0142(197908)44:2⟨763::AID-CNCR2820440251⟩3.0.CO;2-5.